Mon. Not. R. Astron. Soc. **374,** 1479–1494 (2007) doi:10.1111/j.1365-2966.2006.11266.x

Forming disc galaxies in ΛCDM simulations

F. Governato,[1,2⋆] B. Willman,[3] L. Mayer,[4] A. Brooks,[1] G. Stinson,[1] O. Valenzuela,[1] J. Wadsley[5] and T. Quinn[1]

[1]*Department of Astronomy, University of Washington, Box 351580, Seattle, WA 98195, USA*
[2]*INAF, Osservatorio Astronomico di Brera, via Brera 29, 20121 Milano, Italy*
[3]*NYU, Department of Physics, 4 Washington Place, New York, NY 10003, USA*
[4]*ETH, Ramistrasse 101, CH-8092 Zurich, Switzerland*
[5]*Department of Physics and Astronomy, McMaster University, Hamilton, Ontario L88 4M1, Canada*

Accepted 2006 November 3. Received 2006 October 27; in original form 2006 February 20

ABSTRACT

We used fully cosmological, high-resolution *N*-body + smooth particle hydrodynamic (SPH) simulations to follow the formation of disc galaxies with rotational velocities between 135 and 270 km s^{-1} in a Λ cold dark matter (CDM) universe. The simulations include gas cooling, star formation, the effects of a uniform ultraviolet (UV) background and a physically motivated description of feedback from supernovae (SNe). The host dark matter haloes have a spin and last major merger redshift typical of galaxy-sized haloes as measured in recent large-scale *N*-body simulations. The simulated galaxies form rotationally supported discs with realistic exponential scalelengths and fall on both the *I* band and baryonic Tully–Fisher relations. An extended stellar disc forms inside the Milky Way (MW)-sized halo immediately after the last major merger. The combination of UV background and SN feedback drastically reduces the number of visible satellites orbiting inside a MW-sized halo, bringing it in fair agreement with observations. Our simulations predict that the average age of a primary galaxy's stellar population decreases with mass, because feedback delays star formation in less massive galaxies. Galaxies have stellar masses and current star formation rates as a function of total mass that are in good agreement with observational data. We discuss how both high mass and force resolution and a realistic description of star formation and feedback are important ingredients to match the observed properties of galaxies.

Key words: methods: *N*-body simulations – galaxies: evolution – galaxies: formation.

1 INTRODUCTION

In a universe dominated by cold dark matter (CDM) and a cosmological constant (Blumenthal et al. 1984; Bardeen et al. 1986; Peebles & Ratra 2003; Spergel et al. 2003), galaxy formation and evolution is a complex combination of hierarchical clustering, gas dissipation, merging and secular evolution. While gravity drives the bottom-up assembly of cosmic structures (Davis et al. 1985), gas cools at the centres of dark matter (DM) haloes and acquires angular momentum through tidal torques from nearby structures (Fall & Efstathiou 1980; Fall 1983). Cool gas eventually fragments due to Jeans instabilities and forms stars (Peebles 1969; White & Rees 1978). Gravitational interactions between galaxies can instigate star formation (SF) and transform discs into spheroids (Toomre & Toomre 1972) and may dominate galaxy evolution at early epochs especially in dense environments (Frenk et al. 1985). Secular processes, such as external gas accretion or gas displacement due to bars, may play a more important role in galaxy evolution at later epochs (Valenzuela & Klypin 2003; Debattista et al. 2004; Kormendy & Kennicutt 2004). Galaxy formation in this framework is a continuous, ongoing process where the observable properties of galaxies are a function of their merging histories, masses and environments (e.g. Blanton et al. 2003; Shen et al. 2003; Brinchmann et al. 2004; Bundy, Ellis & Conselice 2005).

N-body/gas dynamical simulations have become the primary tools with which to model galaxy formation in a cosmological context. They are necessary to follow the evolution of the internal structure of galaxies as well as the complex interplay between baryon cooling and feedback (Lake & Carlberg 1988; Katz 1992; Navarro & White 1994; Barnes & Hernquist 1996; Quinn, Katz & Efstathiou 1996; Haehnelt, Steinmetz & Rauch 1998; Cen & Ostriker 1999; Mac Low & Ferrara 1999; Navarro & Steinmetz 2000; Thacker & Couchman 2000; Tittley, Pearce & Couchman 2001; Sommer-Larsen, Götz & Portinari 2003; Governato et al. 2004). However, numerical simulations have had difficulties reproducing the properties of real galaxies.

⋆E-mail: fabio@astro.washington.edu

Early work reported a catastrophic loss of angular momentum in the baryonic component of simulated galaxies, leading to the formation of galaxies dominated by a central concentration of cold baryons (Navarro & White 1994). As predicted by early theoretical models (White & Rees 1978; White & Frenk 1991), simulations without strong energy feedback from stellar processes have also suffered from overly efficient SF. This causes galaxies to form most of their stellar component as soon as gas is able to collapse and cool within small haloes, well before the assembly of the main progenitor (Balogh et al. 2001). Dense clumps of stars and cold gas might then spiral rapidly at the centre of the main galaxy due to dynamical friction (Navarro & Steinmetz 1997). These shortcomings resulted in compact galaxies with a central excess of old stars and offset from the observed Tully–Fisher (TF) relation (Giovanelli et al. 1997). The offset was $\sim$1.5 mag for an $\Omega_0 = 1$ CDM cosmology (Navarro & Steinmetz 2000; Eke, Navarro & Steinmetz 2001) and $\sim$0.5 mag in a high σ_8 ΛCDM (Eke et al. 2001).

More recently, attention has been drawn to the 'missing galaxy problem'. DM only simulations predict over an order of magnitude more subhaloes around Milky Way (MW)-like galaxies than the number of dwarfs observed around the MW and M31 (Klypin et al. 1999; Moore et al. 1999; Willman et al. 2004). Observations also show that more massive late-type galaxies have older stellar populations than less massive late-type galaxies (Ferreras et al. 2004; MacArthur et al. 2004; Gallazzi et al. 2005), in possible contradiction with the fact that in CDM scenarios less massive haloes assemble (on average) first.

The angular momentum and missing galaxy problems have often been linked to two major stumbling blocks for numerical galaxy formation: (i) insufficient numerical resolution and (ii) inaccurate treatment of feedback due to SF. Only the most recent gas dynamical simulations have achieved spatial resolution sufficient to resolve the disc scalelengths of discs. Governato et al. (2004) and Kaufmann et al. (2006b) have shown that poor mass and spatial resolution might lead to significant numerical angular momentum loss in baryonic discs embedded in DM haloes. These works suggested that at least 10^5 DM particles (and equivalent numbers in gas and star particles) within the virial radius as well as force resolution of $\leqslant$1 kpc are required to faithfully simulate the formation and dynamical evolution of disc systems over cosmic times. Recent simulations (Abadi et al. 2003; Brook et al. 2004; Robertson et al. 2004; Okamoto et al. 2005) that used a large number of particles and a high force resolution have indeed formed galaxies with extended stellar discs. However, most of the galaxies formed in most of these simulations also had a massive spheroidal component or discs only partially supported by rotation.

The impossibility of directly resolving the scales at which SF and feedback happen (a few pc) makes it necessary to develop simplified models to describe SF and subsequent energy feedback from supernovae (SNe) at galactic scales (0.1–1 kpc; Efstathiou 2000; Silk 2001; Wada & Norman 2001; Ferrara 2002; Krumholz & McKee 2005; Slyz et al. 2005). In early simulations, thermal energy that was simply added to gas surrounding star-forming regions was quickly radiated away, resulting in overcooled gas (Katz 1992). However, heated, diffuse baryons resulting from a proper treatment of feedback may be less susceptible to angular momentum transfer to halo particles (Mo & Miralda-Escude 1996; Eke, Efstathiou & Wright 2000; Maller & Dekel 2002; D'Onghia et al. 2006). To address this shortcoming, Gerritsen (1997), Yepes et al. (1997) and Thacker & Couchman (2000) modelled the pressure support stimulated by gas turbulence by shutting off cooling on time-scales of a few million years, and reported the formation of larger discs. Brook et al. (2004) used a scheme similar to that of Thacker & Couchman (2000) and also found it produced reasonably realistic galaxy discs when applied to simplified cosmological initial conditions. Robertson et al. (2004) used an approach similar to that of Springel (2000) and found that the pressure support produced by their multiphase treatment of the interstellar medium (ISM) was an important factor in the formation of large discs. SN feedback and the ultraviolet (UV) background, being able to reduce gas retention and accretion in haloes with low virial temperature, may also solve the problem of the overabundance of satellites (Quinn et al. 1996; Gnedin 2000; Benson et al. 2002; Dekel & Woo 2003; Kravtsov, Gnedin & Klypin 2004; Monaco 2004). Other recent papers have investigated the roles of a top heavy initial mass function (IMF) (Okamoto et al. 2005) and of massive galaxy outflows driven by quasi-stellar object (QSO) activity (Binney, Gerhard & Silk 2001; Granato et al. 2004; Di Matteo, Springel & Hernquist 2005) in regulating galaxy formation.

In this paper, we study the effect of feedback on the structure and satellites of disc galaxies formed within cosmological haloes spanning a significant mass range (from 10^{12} down to $10^8\,M_\odot$). We improve over previous work in two ways. First, the mass and spatial resolution of these simulations are sufficient to resolve (i) the structure of present day discs without being significantly limited by resolution and (ii) the subhalo population for each galaxy in our sample down to circular velocities of about 20 per cent of their parent halo allowing us study the basic properties of galactic satellites. Second, we use a revised implementation of the SF algorithm introduced by Katz (1992) combined with the feedback recipe introduced by Gerritsen (1997) and then studied by Thacker & Couchman (2000). Details of our implementation can be found in Stinson et al. (2006, hereafter S06). In this paper we calibrate the free parameters of our algorithm to accurately describe the SF in isolated galaxy models of present day galaxies. We then apply this algorithm to cosmological simulations of individual high-resolution galaxies spanning a decade in mass and analyse their properties.

We focus our analysis in this paper on three fundamental properties of present day galaxies.

(i) The abundance and luminosities of galactic satellites.

(ii) The TF and baryonic TF relations (Giovanelli et al. 1997; McGaugh 2005).

(iii) Global star formation histories (SFHs) and $z = 0$ star formation rates (SFRs).

In Section 2, we briefly describe the code and the SF algorithm. A detailed description of our SF and feedback algorithm with additional tests to those presented here is presented in S06. In Section 3, we summarize the cosmological runs performed with a range of feedback algorithms, and in Sections 4–9, we discuss and describe in detail the properties of our simulated galaxies. We plan to explore other aspects of both low and high redshift galaxy formation in future papers.

2 THE CODE AND THE SF ALGORITHM

2.1 Gasoline

We used GASOLINE (Wadsley, Stadel & Quinn 2004), a smooth particle hydrodynamic (SPH), parallel tree code that is both spatially and temporally adaptive with individual time-steps. The version of GASOLINE we used implemented (i) Compton and radiative cooling, (ii) SF and a SN feedback as described in detail in Katz, Weinberg & Hernquist (1996) and S06 and (iii) a UV background following an updated version of Haardt & Madau (1996) (Haardt, private

communication) starting at $z = 6$. The opening angle, θ, was 0.55 until $z = 2$ and 0.75 thereafter, and the time-stepping criterion, η, was 0.2, as in Diemand et al. (2004). The minimum smoothing length allowed is equal to 0.1 times the gravitational softening. Exactly 32 neighbours are used for SPH calculations. An ideal gas of primordial composition is assumed. We calculate the cooling/heating rate and ionization state of each particle by assuming collisional ionization equilibrium and the presence of the time-dependent, but uniform UV background. The code treats artificial viscosity as suggested in Balsara (1997). The energy equation is computed asymmetrically (Evrard 1988; Monaghan 1992; Springel & Hernquist 2002). This approach avoids the energy conservation and negative energy problems of the arithmetic and geometric implementations and converges to the high resolution answer as well as other recently proposed methods (Benz 1990; Springel & Hernquist 2002; Wadsley et al. 2004).

2.2 The SF and SN feedback algorithm

Our SF algorithm can be broken down into three main parts: (i) identifying the star-forming regions, (ii) forming stars and (iii) treating stellar evolution including such effects as mass loss, SN winds and metal enrichment. The algorithm has only three free parameters: $c\star$, ϵSN and β. We define these parameters and summarize the main features of the algorithm below. This algorithm is described in detail in S06.

2.2.1 Criteria for SF

The criteria for a gas particle to become eligible for SF are as follows: (i) its temperature is colder than 30 000 K; (ii) local gas density is higher than 0.1 cm^{-3}; (iii) the gas particle is part of a converging flow measured over the 32 nearest neighbours. We do not require the criterion that gas particles are Jeans unstable (Kawata et al. 2006). A minimum gas overdensity $\delta\rho/\rho$ is also required to avoid spurious SF at very high z. We base the rate at which gas is converted into stars, $\mathrm{d}\rho_\star/\mathrm{d}t$, on the relation

$$\frac{\mathrm{d}\rho_\star}{\mathrm{d}t} = \rho_{\mathrm{gas}}^{3/2}, \tag{1}$$

where ρ represents the volume density. Using the fact that dynamical time, $t_{\mathrm{dyn}} \propto \rho^{-1/2}$, we express this as

$$\frac{\mathrm{d}\rho_\star}{\mathrm{d}t} = c\star\frac{\rho_{\mathrm{gas}}}{t_{\mathrm{dyn}}}, \tag{2}$$

where we have introduced a constant efficiency factor $c\star$ to enable us to calibrate the SF algorithm to match SFRs observed for $z = 0$ galaxies. The mass of star particles formed is fixed to 30 per cent of its parent gas particle initial mass (Okamoto et al. 2005). Once the particle passes the above criteria, to implement equation (1) in a discrete system we assign a probability p that a star will actually be spawned from its parent gas particle:

$$p = \frac{M_{\mathrm{SF}}}{M_{\mathrm{GP}}}\left[1 - \mathrm{e}^{-(c\star\Delta t)/(t_{\mathrm{form}})}\right], \tag{3}$$

where we have introduced M_{SF}, the spawning mass for star particles, M_{GP}, the mass of the gas particle that is creating the star, Δt, the SF time-scale (1 Myr in all of the simulations described in this paper) and t_{form}, which is either the dynamical time or the cooling time, whichever is longer. Gas particles in dense regions with shorter dynamical times will form stars at a higher probability.

2.2.2 Feedback and metal enrichment from SNe

Our implementation of feedback qualitatively follows the algorithm implemented by Thacker & Couchman (2000). We assume that the energy released into the ISM turns into turbulent motions (at unresolved scales) and is partially dissipated, preventing the gas from cooling and forming stars. We determine the number of Type Ia and II SN that occur during each time-step from Raiteri, Villata & Navarro (1996) using a Miller–Scalo IMF and the stellar lifetimes of stars. We then multiply the number of both SN types that explode by a fraction of the canonical 10^{51} erg/SN times a fixed efficiency term (ϵSN), and distribute that energy to the surrounding gas particles. In Section 2.3.2, we explore efficiency values in the range 0.1 to 0.6. At an efficiency $\epsilon\mathrm{SN} = 0.1$ and with the adopted IMF, 7.65×10^{47} erg of energy are deposited into the surrounding gas for every one $\mathrm{M}_\odot$ of star formed. Energy is distributed using the smoothing kernel over the 32 nearest neighbour particles. In our algorithm the time-scale for the cooling shut off and the amount of mass affected are physically motivated and chosen following typical values from the McKee & Ostriker (1977) and Ostriker & McKee (1988) blast wave model. When energy injection comes from a SN II event we disable the radiative cooling for 30 Myr in a number of the nearest neighbour particles that satisfy

$$\beta M_{\mathrm{SN\,II}} > \frac{4\pi r^3}{3}\rho_{\mathrm{ave}}, \tag{4}$$

where $M_{\mathrm{SN\,II}}$ is the mass of SNe produced in a star in a given time-step, r is the distance from the star to the gas particle in question, ρ_{ave} is the local gas density and β is a normalization factor. In Section 2.3.2, we explore β values in the range 0.05 to 0.2. For each SF event the maximum number of particles that can have the cooling disabled as from equation (4) is the number of SPH neighbours (32 in our simulations).

Once formed, we treat each star particle as a single stellar population with uniform metallicity. The code also keeps track of mass loss from stellar winds. With the adopted IMF, star particles lose up to 30–40 per cent of their original mass as their underlying stellar population ages. This mass gets distributed to nearby gas particles. Metals come from both SNe Ia and II. Metal enrichment follows Raiteri et al. (1996). Like energy, metals are distributed using the smoothing kernel over the 32 nearest neighbour particles. We plan to study the metallicity of the baryonic component of our simulated galaxies and to introduce metal lines cooling in future papers.

2.3 Using isolated galaxy models to calibrate the SF and SN feedback algorithms

We performed a number of simulations of isolated in equilibrium galaxy models to study the effect of different combinations of the three free SF parameters ($c\star$, β and ϵSN) on the properties of galaxies with a quiescent SF and over a range of masses. Parameters were varied within a range of plausible values suggested by observational constraints. The SF efficiency parameter $c\star$ was varied over the range (0.01–0.4), the mass factor β over (0.05–0.4) and the SN efficiency ϵSN in the range (0.1–0.6); see Table 1. This is a subset of the parameter space explored in S06 where tests were focused on a MW-sized galaxy. However, it is important to extend tests to less massive galaxies. Hence in this work we followed a complementary approach, focusing on the properties of a much smaller galaxy and then verifying that the best parameters so identified would model realistically SF in a MW-sized halo.

Table 1. Summary of the properties of some of the isolated dwarf runs for a given set of $c\star$, β and ϵSN parameters. SFR is measured over the whole disc after it has set to a quasi-steady rate. $\sigma_{\rm gas}$ and $\sigma_{\rm star}$ (the azimuthal velocity dispersions) and $R_z/R_{\rm d}$ are measured at two stellar disc scalelengths. The volume ratio of the hot gas ($T > 10^5$ K) and cold gas included all gas particles within 2 kpc from the disc plane.

Run	$c\star$	β	ϵSN	SFR ($M_\odot$ yr^{-1})	$\sigma_{\rm gas}$ (km s^{-1})	$\sigma_{\rm star}$ (km s^{-1})	$R_z/R_{\rm d}$	Hot/cold gas volume ratio
DWFiso01	0.05	0.05	0.1	0.20	12	12	0.23	0.5
DWFiso02[a]	0.05	0.05	0.2	0.16	14	14	0.31	0.6
DWFiso03[a]	0.05	0.05	0.4	0.12	17	16	0.22	0.6
DWFiso04[a]	0.05	0.05	0.6	0.06	35	22	0.27	0.9
DWFiso05	0.20	0.05	0.2	0.18	22	20	0.43	1.0
DWFiso06	0.20	0.10	0.2	0.15	20	16	0.61	1.5
DWFiso07	0.20	0.20	0.2	0.13	18	20	0.5	2.0
DWFiso08	0.20	0.20	0.6	0.03	36	28	0.84	1.6

[a]Parameters used for the cosmological runs.

2.3.1 *The galaxy models*

To explore the effects of our feedback recipe we applied it to two galaxy models having different peak circular velocities: 220 (MWiso) and 70 km s^{-1} (DWFiso), respectively (where iso stands for 'isolated'). Both models were built as equilibrium configurations using the procedure outlined in Springel (2000). Rather than trying to model specific galaxies, we built models consistent with the trend for smaller galaxies to have smaller bulge components and a larger cold gas fraction in the disc (McGaugh 2005; West et al. 2005). The models include a rotationally supported stellar and gaseous disc, a bulge for the MW model only and a DM halo component extending to the virial radius. Stars start with a Toomre parameter $Q = 2$. Discs are built to be stable to bar instabilities.

The dwarf galaxy has no bulge component and gas contributes 50 per cent to its total disc mass. 10^5 particles are in its DM halo, and 1.5×10^4 gas and 2×10^4 star particles are in its disc. The softening length is set to about 0.2 times the disc scalelength ($R_{\rm d} \sim 1$ kpc). Gas and stars have the same exponential radial distribution. Because of its relatively shallow potential, we expect this galaxy to be fairly sensitive to the details of the feedback and SF algorithm.

Our MW model (MWiso, the same as in S06) has the structural parameters outlined in Klypin, Zhao & Somerville (2002), so providing an excellent fit to the existing data of the matter distribution in our own Galaxy. Our MW disc is modelled by 4.5×10^4 star particles and 10^4 gas particles with a softening of 325 pc. This resolution is similar to that of our cosmological runs. The stellar bulge to disc ratio is 1:7, and gas contributes about 10 per cent of the total mass in the disc component. Disc scalelengths are 3.5 and 7 kpc, respectively, for stars and gas (Broeils & Rhee 1997).

2.3.2 *Comparison between models and observations*

A set of 25 runs allowed us to study in more detail the effect of the three free parameters ($c\star$, β and ϵSN) in our SF algorithm on the properties of the DWFiso model. In this section, we highlight the main trends of simulated galaxy properties with each of the three parameters to motivate our best choice parameters.

Table 1 summarizes the results of eight representative DWFiso runs. The parameters used in these eight runs all produce galaxies with SFRs that range between 0.03 and 0.20 $M_\odot$ yr^{-1} and have velocity dispersions of their cold ($T < 30\,000$ K) gas component that range between 12 and 36 km s^{-1}. These values are all consistent with those observed for nearby dwarf galaxies, aside from the two galaxies (ϵSN = 0.6) with the largest $\sigma_{\rm gas}$. The SFR measured from the Sloan Digital Sky Survey (SDSS) (Brinchmann et al. 2004) for small galaxies with stellar masses around 10^9 $M_\odot$ ranges typically between 0.02 and 0.5 $M_\odot$ yr^{-1} and has a median value of 0.2–0.3 $M_\odot$ yr^{-1} (Brinchmann et al. 2004). Observed values for the velocity dispersion of the cold gas component in discs range in the 10–30 km s^{-1} range (Pizzella et al. 2004) (see Fig. 1).

Although all of the representative runs produce reasonable SFRs and $\sigma_{\rm gas}$, only runs with low $c\star$ (0.05 in the representative sample) produce discs that are thin enough to match observations. The observed ratio of the stellar disc scaleheight (R_z) to stellar disc scalelength ($R_{\rm d}$) is usually in the range 0.25–0.33 for normal disc galaxies (Bizyaev & Mitronova 2002). We find that values of $c\star$ larger than 0.05 tend to form 'thick' discs with a $R_z/R_{\rm d}$ ratio larger than observed, possibly because more stars are allowed to form in regions further away from the disc plane. The $R_z/R_{\rm d}$ ratio is only weakly dependent on ϵSN or β (runs 1 through 4, 5, 6 and 7 in Table 1). This suggests that at our resolution low values of $c\star$ should be preferred to obtain thinner discs. Tests in S06 show $c\star$ to be weakly dependent on resolution when at least a few tens of thousands gas + star particles are used. However, higher $c\star$ values have been used when star-forming regions are individually resolved (Tasker & Bryan 2006).

As the β factor is increased, more gas is affected by feedback and the volume ratio of the hot/cold phases increases (runs 6, 7 and 8 in Table 1). In our tests we found that runs with the required low values of $c\star$ tend to form and maintain a large bubble of hot gas in the central region of our models, locally inhibiting SF, unless β is also low. We thus excluded the region of parameter space with $\beta > c\star$ from our analysis as being unrealistic.

Fig. 2 shows how the gas spatial distribution of the DWFiso model is affected as $c\star$ and β are fixed to their desired value of 0.05 and ϵSN is varied from 0.1 to 0.6. In the DWFiso runs, higher ϵSN leads to lower SFRs and a higher cold gas turbulence (e.g. runs 3, 4 and 8). The SFR of the dwarf galaxy model is most sensitive to the SN energy efficiency parameter ϵSN, with a realistic SFR obtained with values in the range 0.1–0.6. The images in Fig. 2 show that large SN efficiency values create a 'galactic fountain' and a patchy gas distribution on the disc plane resembling that of observed small galaxies. However, even with $\epsilon = 0.6$ only a very small fraction of the gas ejected from the disc plane becomes unbound from the DM halo, in agreement with observational evidence and some theoretical expectations (Mac Low & Ferrara 1999; Martin 1999; Mayer & Moore 2004; McGaugh 2005).

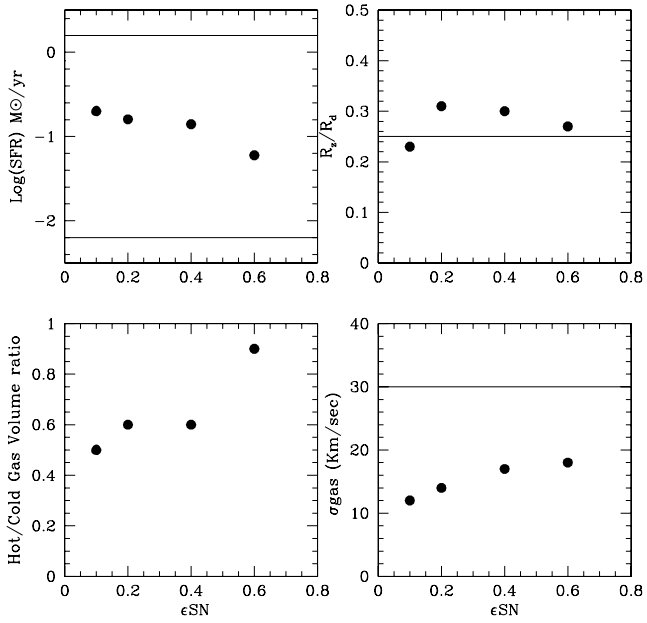

Figure 1. Properties of the dwarf galaxy model as a function of ϵSN. The efficiency parameter $c\star$ and the mass factor β have both been set to 0.05. Upper left: SFRs. The two horizontal lines shows the 95 per cent contour for galaxies of stellar mass $10^{10}\,M_\odot$ from the SDSS (Brinchmann et al. 2004). Upper right: disc scalelength R_d versus the disc scaleheight R_z. The horizontal line is the typical value from Bizyaev & Mitronova (2002) and Yoachim & Dalcanton (2006). Lower left: the hot/cold gas volume ratio as a function of ϵSN. Lower right: cold gas velocity dispersion. The horizontal value is the upper value of $\sigma_{\rm gas}$ from Pizzella et al. (2004).

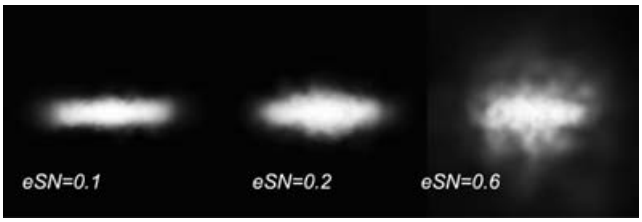

Figure 2. The gas projected density for the dwarf galaxy model seen edge on as ϵSN is varied. The box is 20 kpc across.

Tests on the MWiso model in S06 preferred values of $c\star$ in the 0.01–0.1 range but did not constrain ϵSN significantly due to the relatively deep potential. For the MWiso model we set both $c\star$ and β to 0.05 and varied ϵSN in the range 0.1–0.6 (Table 2). As in S06 the effect of injecting more energy into the ISM is much smaller than for DWFiso, due to the deeper potential well. Increasing ϵSN by a factor of 6 has a small effect on the properties of the ISM, with $\sigma_{\rm gas}$, and the hot/cold gas volume ratio roughly doubling. A smaller 'galactic fountain' is created, but only a small fraction of the gas is ejected away from the disc and none actually leaves the boundaries

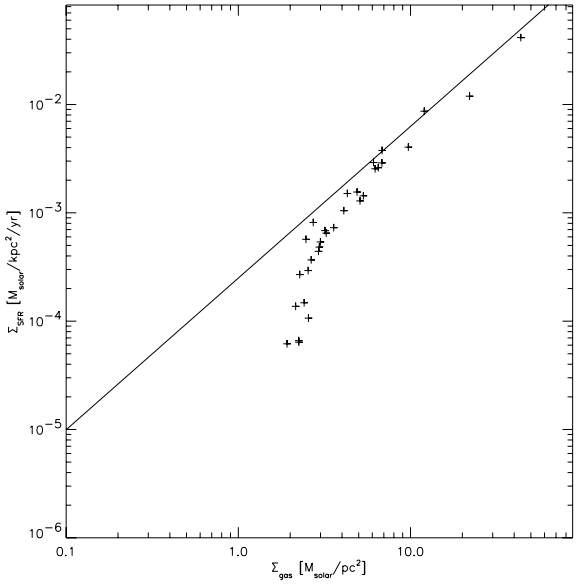

Figure 3. SFR versus local gas surface density. Dots from the MWiso3 galaxy model run (ϵSN = 0.6). The straight line is a fit to Kennicutt's law.

of the surrounding DM halo. The vertical velocity dispersion of the stellar disc increases slightly while the SFR decreases by less than 20 per cent across the whole disc. Disc galaxies over a range of stellar masses show a remarkably tight relation between the gas surface density $\Sigma_{\rm gas}$ and the local surface density of SF, $\Sigma_{\rm SFR}$. Equation (4) of Kennicutt (1998) (originally formulated for the average properties of individual galaxies) states the exact form of this relationship:

$$\Sigma_{\rm SFR} = (2.5 \pm 0.7) \times 10^{-4} \left(\frac{\Sigma_{\rm gas}}{1\,{\rm M}_\odot\,{\rm pc}^{-2}} \right)^{1.4\pm0.15} {\rm M}_\odot\,{\rm yr}^{-1}\,{\rm kpc}^{-2}. \quad (5)$$

As expected from the formulation of equation (5) (Kravtsov & Gnedin 2005), SF across the whole disc of our MWiso models follows closely the slope of the observed Kennicutt's law and is shown in Fig. 3. Increasing ϵSN lowers the SFR normalization slightly, again in agreement with the finding from S06.

To summarize the set of tests described in this section shows that our SF + SN feedback scheme provides a reasonable match to some of the basic properties of present day, isolated galaxies: Kennicutt's law, the observed SFR of galaxies, the turbulence of cold gas (at scales of a few kpc) and the thickness ratio of stellar discs. This provides us with some confidence that our simple scheme is able to capture the important aspects of SF and its effects on the ISM of galaxies over a significant range of masses. There is some degree of interplay between the parameters that could be completely captured only by an even larger set of tests. However, it is clear that within the range of parameters explored in S06 and here, ϵSN predominantly regulates the SFR and the turbulence of the gas. β has to be relatively small to avoid unwanted artificial effects and $c\star$ plays a relevant role

Table 2. Summary of the properties of the isolated MW runs: quantities defined as in Table 1.

Run	$c\star$	β	ϵSN	SFR ($M_\odot\,yr^{-1}$)	$\sigma_{\rm gas}$ ($km\,s^{-1}$)	$\sigma_{\rm star}$ ($km\,s^{-1}$)	R_z/R_d	Hot/cold gas volume ratio
MWiso1	0.05	0.05	0.1	0.85	12	13	0.04	0.22
MWiso2	0.05	0.05	0.4	0.8	18	20	0.05	0.26
MWiso3	0.05	0.05	0.6	0.7	20	24	0.05	0.4

in creating 'thin' stellar discs. Given all of the above considerations we have chosen to run our cosmological simulations keeping $c^\star$ and β fixed at 0.05 while varying ϵSN in the range 0.2–0.6.

3 COSMOLOGICAL RUNS

For our cosmological runs we selected three galaxy-sized haloes (DWF1, MW1 and GAL1) from 28.5- and 100-Mpc boxes, low resolution, DM only simulations run in a concordance, flat, Λ-dominated cosmology: $\Omega_0 = 0.3$, $\Lambda = 0.7$, $h = 0.7$, $\sigma_8 = 0.9$, shape parameter $\Gamma = 0.21$ and $\Omega_b = 0.039$ (Perlmutter et al. 1997). Given the masses and virial radii of the selected haloes the sizes of the starting boxes are large enough to provide realistic torques. The power spectra to model the initial linear density field were calculated using the CMBFAST code to generate transfer functions (Zaldarriaga & Seljak 2000). These three haloes were resimulated at higher resolution using the volume renormalization technique (Katz & White 1993).

We resimulated DWF1, MW1 and GAL1 to have a similar dynamical range in each simulation. Each galaxy model was resimulated to have a similar number of particles within the virial radius, and the softenings were rescaled so that the spatial resolution of each galaxy was a similar fraction of its virial radius. With our choices of particle number and softening, the smallest subhaloes resolved have typical circular velocities of 20 per cent of their host. For all particle species in the high-resolution region, the gravitational spline softening, $\epsilon(z)$, evolved comovingly from the starting redshift ($z \sim 100$) until $z = 9$, and remained fixed at their final value from $z = 9$ to the present. The softening values chosen are a good compromise between reducing two body relaxation and ensuring that disc scalelengths and the central part of DM haloes will be spatially resolved (see Diemand et al. 2004 for a number of relevant tests). Integration parameter values were chosen as suggested in Moore et al. (1998) and then confirmed in Power et al. (2003).

We selected a halo mass range to study haloes associated with typical disc galaxies. The three selected haloes have masses of 1.6×10^{11} (DWF1), 1.15×10^{12} (MW1) and $3.1 \times 10^{12}\,M_\odot$ (GAL1) measured within their virial radius R_{vir} (the radius enclosing an overdensity of 100 times the critical density ρ_{crit}). GAL1, the largest halo, is more massive than that of our MW, as a recent analysis points to a MW halo of about $10^{12}\,M_\odot$ (Klypin et al. 2002). This is the mass of our intermediate size halo (MW1). Our least massive halo, DWF1, corresponds to that of a typical disc field galaxy. The three galaxies span a range of circular velocities V_c (measured at R_{vir}) and defined as $\sqrt{M(r < R)/R}$ between 70 and 185 km s^{-1}. Note that this V_c is defined differently than the V_{rot} used later in the paper. DM particle masses in the high-resolution regions were 7.6×10^5, 6.05×10^6 and $2.3 \times 10^7\,M_\odot$ and the spline softening was 0.3, 0.6 and 1 kpc for DWF1, MW1 and GAL1 runs, respectively. The MW1 halo was also run at higher resolution to test resolution effects. The results of the resolution testing are in Section 8. GAL1 is the same halo described in Governato et al. (2004). The main halo properties are summarized in Table 3.

The merging histories and angular momentum of parent DM haloes play a major role in defining the final properties of the galaxies that form inside them (Cole et al. 2000). It is therefore important to make sure that our haloes have merging histories and spin parameters somewhat representative of the global population. The three galaxies were selected with the only criteria of the redshift of their last major merger (z_{lmm}) > 2 and with no haloes of similar or larger mass within a few virial radii. A major merger is defined here as having a 3:1 mass ratio. The three haloes have formation times (defined as the main progenitor achieving 50 per cent of its final mass) in the 0.6–1.5 redshift range. Their spin parameter, λ (defined as $JE^{1/2}/GM^{5/2}$), varies from 0.01 for DWF1 to 0.05 for MW1, with the average value for cosmic haloes $\sim$0.035 (Gardner 2001).

z_{lmm} is likely a crucial parameter in defining the properties of a galaxy disc (Steinmetz & Navarro 2002). If mergers efficiently destroy discs, a low z_{lmm} would leave less time to grow a new stellar disc from newly accreted gas (Baugh, Cole & Frenk 1996). We therefore stress that the z_{lmm} of these three haloes is close to the average of the population of galaxy-sized haloes in our adopted cosmology, as measured in a recent large set of N-body simulations (Li, Mo & van den Bosch 2005). The same authors showed that previous estimates of the average z_{lmm} estimates based on the extended Press & Schechter approach were biased towards lower z's. DWF1 has its last major merger at $z = 2.3$, when a head-on encounter generates a very prolate halo. It only accretes relatively small haloes after that. After its last major merger at $z = 2.5$, MW1 has a counter rotating minor merger at $z = 2$. A relatively high z_{lmm} for the MW1 halo is consistent with the MW forming several Gyrs ago (Gilmore, Wyse & Norris 2002). At $z = 2.75$, GAL1 undergoes multiple mergers and accretes several satellites after that. A few get disrupted after several passages through its disc. In the future, we plan to simulate the formation of galaxies with a wider range of initial conditions.

For each halo a sequence of runs of increasing complexity was performed. Table 4 summarizes these runs. For the MW halo initial conditions, we performed the following runs: DM only (MW1dm), no gas cooling or SF (MW1ad), no feedback and no UV (MW1g0), UV turned on but without stellar feedback (MW1g1) and three runs with various SN efficiencies (MW1g2 to MW1g4). In all runs with SF we kept the SF efficiency and the mass factor β fixed and varied only the fraction of energy from SN dumped into the ISM (ϵSN) from 0.2 to 0.6. Based on the results from Section 2 we will mainly focus on the properties of the runs with a SN energy efficiency of 40 per cent (ϵSN $= 0.4$). Results from the cosmological runs confirm a posteriori this choice: a higher SN efficiency creates a DWF1 galaxy with an unrealistic low cold gas mass fraction in the disc (<3 per cent).

Table 3. Summary of the properties of the three cosmological haloes.

Run	Virial mass ($M_\odot$)	Virial radius (kpc)	V_c [a] (km s^{-1})	Formation time (z)	λ	Last major merger (z)	ϵ (kpc)	N_{tot} [b] at $z = 0$ (dark+gas+stars)
DWF1	1.6×10^{11}	142	70	1.5	0.01	2.3	0.3	$\sim$860.000
MW1	1.15×10^{12}	271	134	0.6	0.07	2.5	0.6–0.3[c]	$\sim$700.000–4.000.000[c]
GAL1	3.1×10^{12}	380	185	0.96	0.035	2.75	1.0	$\sim$480.000

[a] Circular velocity at virial radius.
[b] Number of gas and star particles changes slightly depending on ϵSN.
[c] Smaller/larger values are for the $z = 0.5$ super high resolution run, respectively.

Table 4. Main parameters of cosmological galaxy runs.

Run	$c\star$	β	UV	ϵSN
DWF1g1	0.05	–	Off	Off
DWF1g2	0.05	0.05	On	0.4
DWF1g3	0.05	0.05	On	0.6
MW1dm	DM only			
MW1ad	No SF, no cooling			
MW1g0	0.05	–	Off	Off
MW1g1	0.05	0.05	On	Off
MW1g2	0.05	0.05	On	0.2
MW1g3	0.05	0.05	On	0.4
MW1g4	0.05	0.05	On	0.6
MW1hr	0.05	0.05	On	0.6
GAL1g1	0.05	0.05	On	Off
GAL1g2	0.05	0.05	On	0.2
GAL1g3	0.05	0.05	On	0.4

Our MW1g4 (ϵSN $= 0.6$) run of the MW1 halo was repeated at eight times better mass resolution and two times better spatial resolution (run MW1hr in Table 4). The run was stopped at $z = 0.5$ due to its computational cost. With four million resolution elements within the virial radius, a star particle mass of 3×10^4 M$_\odot$ and a force resolution of 0.3 kpc, this run has likely the highest resolution ever achieved for a MW-sized galaxy simulation carried to a relatively small redshift. We will use this simulation to test the effects of increasing resolution in Section 8.

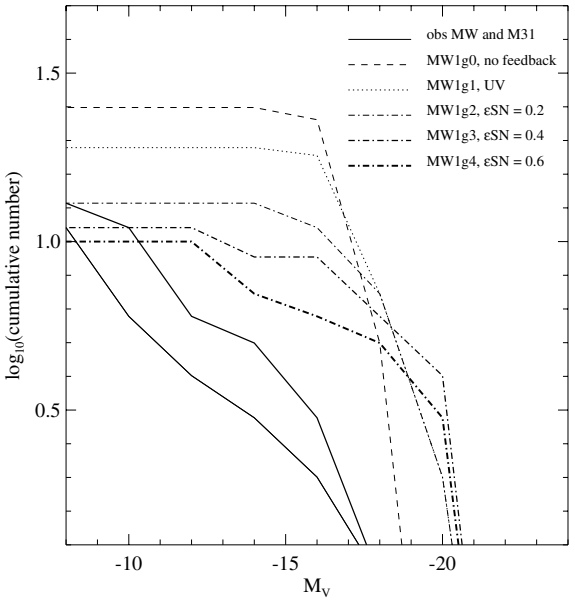

Figure 4. The LFs of satellites within $R_{\rm vir}$ in all four MW1 runs, compared with the LFs of both the MW's and of M31's satellites. Only satellites containing at least 64 DM particles are included. The two runs without SN feedback produce far too many satellites. However, all three of the runs including SN feedback produce a number of satellites that reasonably matches that of the MW and M31 satellite populations (lower and upper solid lines, respectively), although the simulated satellites are still too bright.

4 THE EFFECT OF FEEDBACK ON THE PROPERTIES OF SATELLITES

To explore the effect of UV and SN feedback on satellites, we compare the properties of satellites within the virial radius in the six MW1 simulations described in Table 4. The MW1 satellites are the most easily comparable to the satellites of our own MW (Mateo 1998). Unless specified, similar qualitative conclusions apply to DWF1 and GAL1. We will present a much more detailed analysis of the satellites in a subsequent paper. Subhaloes were identified using SKID (Governato et al. 1997) and only those with at least 64 DM particles were used in the analysis. That minimum number of DM particles translates to minimum DM masses of 0.49, 3.9 and 14.9×10^8 M$_\odot$ for the satellites of DWF1, MW1 and GAL1, respectively. The resolution limit translates into a circular velocity limit of $V_{\rm c} \sim$ 20–30 km s^{-1} depending on the individual satellite density profile. We use the ages and metallicities of each star particle in the satellites to determine their absolute V-band magnitudes assuming no dust reddening. Satellites have a mean (not luminosity weighted) $B-V$ of 0.63. We verified that field dwarfs have slightly bluer colours.

Fig. 4 shows the satellite luminosity functions (LFs) of the MW1 cosmological runs compared with those observed for the MW and M31. A comparison of both the g0 and g1 simulations (no feedback; then UV on, but no SN feedback) with the observed satellite LFs of the MW and M31 highlights the missing satellite problem. On the contrary, runs including SN feedback result in satellite populations similar in number, although not in luminosity, to the observed populations. The total number of luminous satellites is not strongly dependent on the strength of feedback implemented in the S06 algorithm.

Although both g0 and g1 have a total of 26 satellites, the runs including SN feedback all have 20 or fewer satellites total, only some of which host stars. This difference in total satellite number occurs because simulations with more severe overcooling form satellites very centrally concentrated and less susceptible to tidal effects and complete disruption (see also Macciò, Governato & Horellou 2005). Similarly, runs with cooling but no SN feedback (as MW1g0 and MW1g1) contain $\sim$2$\times$ the number of satellites as the DM only run or the run with no gas cooling.

Fig. 5 shows that some of the satellites in the runs including UV are completely devoid of stars. There are no satellites within $R_{\rm vir}$ in any of the simulations that retain gas but do not contain any stars. Unlike UV feedback, SN feedback can also expel gas from the satellites once they start forming stars, reducing the overall baryon fraction of satellites containing stars. These reduced baryon fraction satellites are seen in Fig. 5. As expected, the satellites of the run with stronger SN feedback have a smaller baryon fraction than the run with weaker SN feedback. The LFs of satellites in the MW1 (and of GAL1) simulations show that the introduction of SN feedback in particular is essential to reproduce the observed number of satellites in MW-type galaxies. The number of satellites containing stars appear is fairly robust as resolution is increased (see Fig. 20). At a higher resolution while tens of less massive dark satellites are resolved, only a few more are able to make stars. This is because the mass threshold below which the UV field makes satellites completely dark (Quinn et al. 1996) is resolved in our runs (Fig. 5). All but one satellite of galaxy DWF1 (the run with the best mass resolution in our set) are completely dark when SN feedback is on. Note that the list of known MW satellites at very low luminosities and surface brightnesses might still be incomplete (see Willman et al. 2004 for a discussion).

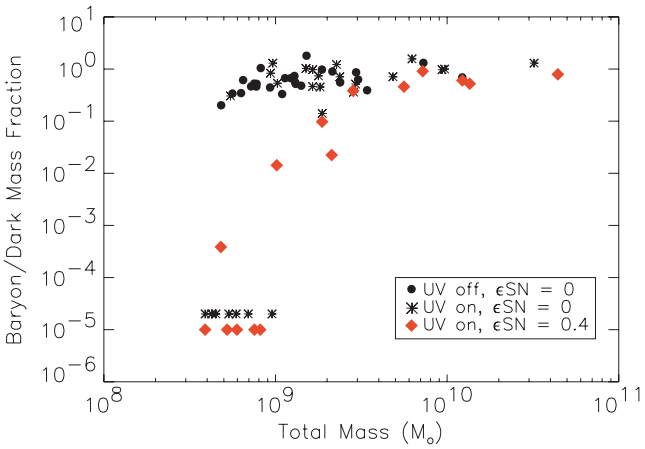

Figure 5. The baryon to DM ratio for all the subhaloes within $R_{\rm vir}$ of the MW1 galaxy. With no UV field or SN feedback the baryon fraction is constant down to our resolution limit of 64 DM particles. UV creates some dark satellites, while SN feedback removes a substantial fraction of baryons from haloes with total masses below a few times 10^9 M$_\odot$. Note that total satellites masses have been affected by tidal stripping. Haloes with no baryons in the UV only run have been shifted upward for clarity.

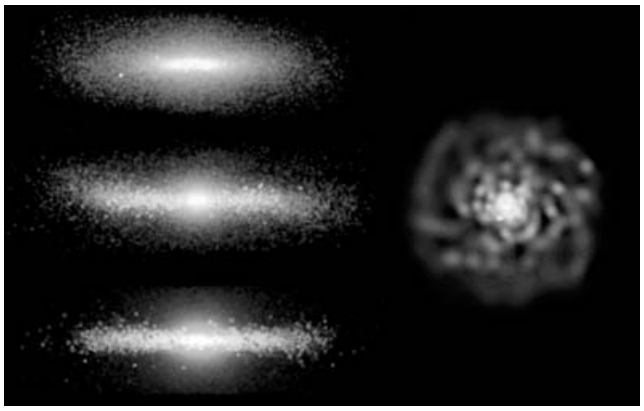

Figure 6. Left-hand panel: brightness maps of the edge-on discs of (from top to bottom) GAL1, MW1 and DWF1 at $z = 0$. Each star particle in the simulations has been weighted by its age-dependent bolometric luminosity. Right-hand panel: the face-on surface density of the gas for DWF1 at $z = 0$. Each frame is 30 kpc across.

5 PROPERTIES OF THE DISCS

The images in Fig. 6 show that all three galaxies have formed a significant stellar disc by redshift $z = 0$. In this section, we discuss in detail the spatial and kinematic properties of the discs, investigate the effects of feedback on disc properties and demonstrate the formation of the discs during major, gas-rich mergers.

5.1 Density profiles of the discs

The top panel of Fig. 7 shows the $z = 0$ stellar surface density profiles of the discs as a function of radius for our fiducial runs (DWF1g2, MW1g3, GAL1g2 – ϵSN = 0.4). Hereafter we will simply refer to these specific runs as DWF1, MW1 and GAL1 as we report and discuss our results. We include all stars within four disc scaleheights, R_z. The stellar disc component of all galaxies is well fit by an exponential distribution between one and three disc scalelengths. The profiles in Fig. 7 illustrate that all galaxies also

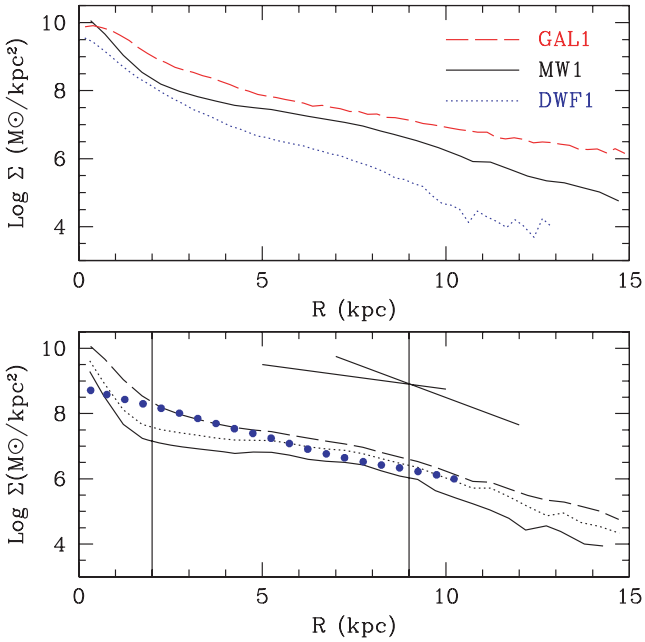

Figure 7. The face-on stellar density profile of the three simulated galaxies. Only stars within $4R_z$ from the disc plane are considered. The upper panel shows the contribution from all stars with a cosmic age between 0 and 10 Gyr, roughly corresponding to the *K* band (Martin et al. 2005). The lower panel shows the projected stellar density profile of the MW1 galaxy for stars in the 0–3 Gyr (solid), 0–4 Gyr (dotted) and 0–10 Gyr (dashed) age range. Dots show the stellar profile of the MW1hr at $z = 1.7$. The two straight lines show the slope of the younger stellar component inside and outside the break radius.

show evidence for a central, steeper component that extends to 1 or 2 kpc.

Disc scalelengths, $R_{\rm D}$, were measured by fitting an exponential profile to the disc component, but excluding the steep central component and stopping where the surface density shows a break. To approximate the effect of measuring the disc scalelength in different optical bands, we measured the scalelengths of stars in different age ranges, <2, <4 and <11 Gyr, to approximate the *B*, *R* and *K* optical bands, respectively (Martin et al. 2005). These scalelengths are summarized in Table 5. The bottom panel of Fig. 7 shows the stellar density profiles of MW1 in each of these three stellar age ranges. Beyond 2.5–3 scalelengths (shown by the outer vertical line), the disc surface density declines rapidly for the youngest stars. These disc profiles are quite common in observed spiral galaxies (Florido et al. 2001; Trujillo & Pohlen 2005). In the remainder of this section we will refer mostly to stars younger than 4 Gyr (*R* band) to illustrate our results, unless otherwise specified.

The exponential disc component forms from the inside out as observed in many disc galaxies (Ryder & Dopita 1994). However, gas inflow due to the late formation of a bar or an oval-like structure in the central few kpc, which is responsible for the observed central steepening of the profile, can trigger enhanced SF in the inner disc, which then forms partially outside in. This mode of disc formation is significant in run GAL1 and was already reported in Governato et al. (2004). At $z = 0$, SF in GAL1 is primarily concentrated in the inner parts of the disc. The scalelength of stars younger than 2 Gyr in GAL1 is only 1.1 kpc, half that of the older component. This is typical of massive S0/early-type disc galaxies (Pohlen et al. 2004).

Table 5. Summary of the properties of the discs of the galaxies formed in the cosmological runs (only runs with ϵSN = 0.4 are shown).

Run	R_{d_B}	R_{d_R}	R_{d_K}	R_{z_R}	$R_{d_{gas}}$	$R_{z_{gas}}$	B_{tot}	I_{tot}	K_{tot}	SFR[a] ($M_\odot$ yr^{-1})	V_c [b]	$M\star$
DWF1	2.02	1.95	1.2	0.3	7.0	0.4	−19.8	−21.2	−22.6	0.6	160	1.38×10^{10}
MW1	4.5	3.8	2.1	1.0	10	1.0	−21.1	−22.6	−24	2.2	205	4.6×10^{10}
GAL1	1.1	1.2	2.15	2.3	6.0	1.3	−22.0	−23.5	−24.9	7.1	180	1.36×10^{11}

[a]At $z = 0$.
[b]At $2.2R_d$.

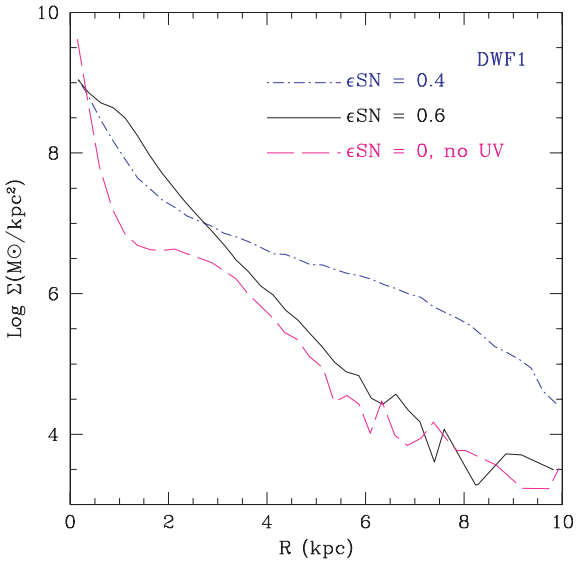

Figure 8. The face-on stellar density profile of the DWF1 galaxy as a function of feedback strength. Only stars within $4R_z$ from the disc plane and in the 0–4 Gyr age range are plotted.

All three galaxies have extended discs of gas colder than a few 10^4 K with exponential scalelengths larger than even the youngest stellar disc component, as in Ryder & Dopita (1994). The right-hand panel of Fig. 6 shows that at our sub-kpc resolution and with our feedback scheme we are able to qualitatively capture the complex nature of the ISM. The gas distribution in the disc plane of our smallest galaxy (DWF1) and in the high resolution MW (MW1hr) shows a complex structure of spiral arms linked by filaments and surrounded by a hotter medium.

The stellar profile of the final discs in the more massive galaxies (MW1 and GAL1) is only weakly dependent on the strength of SNe feedback as we allow the energy efficiency to vary only by a factor of 3, being constrained by the early tests we carried in Section 2. Okamoto et al. (2005) showed how the density distribution might depend substantially on the feedback adopted. It is likely that the energy injection per unit mass in the feedback scheme adopted by Okamoto et al. is higher than in our simulations. Instead, the disc stellar profile of DWF1, our less massive galaxy, is more affected when varying the amount of SN feedback in the same range (Fig. 8). When ϵ increases to 0.6 the stellar density profile of younger stars in DWF1 is best described by a single, exponential profile with a shorter scalelength and truncated at about $2\,R_d$. Similarly to the tests performed in Section 2 the cold gas is much more turbulent, making SF inefficient at low densities. When feedback is turned off cold gas settles in a smaller, more compact disc that originates a denser central core. As the disc surface density increases the disc becomes bar unstable redistributing the stellar material and originating the 'flat' stellar profile at ∼2 kpc that is usually associated with strong dynamical instabilities (Debattista et al. 2006). In all three galaxies runs without feedback form 'hotter' stellar discs with a higher scalelength.

5.2 Kinematics of the discs

We first studied the dynamical properties of the simulated objects and verified that the discs are indeed supported by rotation. For every star particle within the 'disc' we computed J_z, the component of angular momentum parallel to the total angular momentum of all disc stars. We defined the disc stars as those within four (R band) scalelengths and heights centred on each galaxy. We compared J along the z-axis to the angular momentum of the corotating circular orbit with similar orbital energy, $J_c(E)$. Stars in a disc component completely supported by circular motions should by definition have $J/J_c = 1$. Fig. 9 shows the mass weighted distribution for all the disc star particles (left-hand panel) and for disc star particles formed in the last 3 Gyr (right-hand panel). The histogram distributions show clearly that in all three galaxies the disc component is mostly supported by rotation. Our DWF1 and MW1 galaxy models have a higher fraction of stars on circular orbits when compared with the distributions showed by Abadi et al. (2003) and Okamoto et al. (2005). In particular the young stellar component is heavily dominated by stars on almost circular orbits: 80 per cent of young

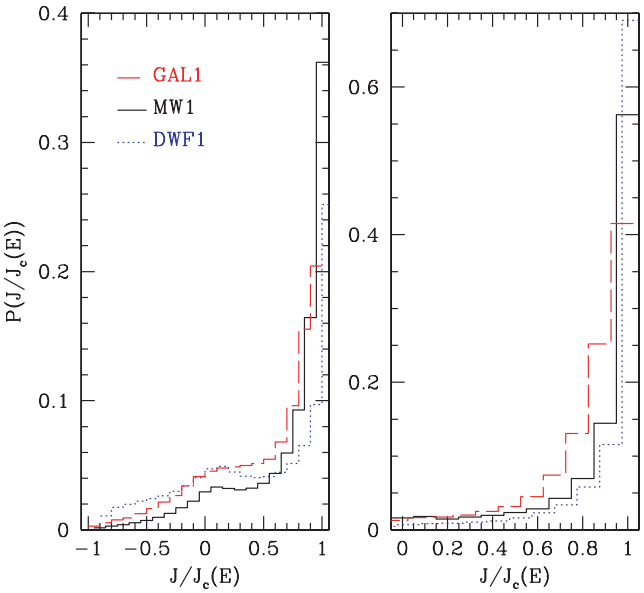

Figure 9. Mass weighted probability distributions of the orbital circularity J/J_c for disc stars in DWF1 (solid), MW1 (dotted) and GAL1 (dashed). The right-hand panel (note the change of scale) shows only star particles formed in the last 3 Gyr.

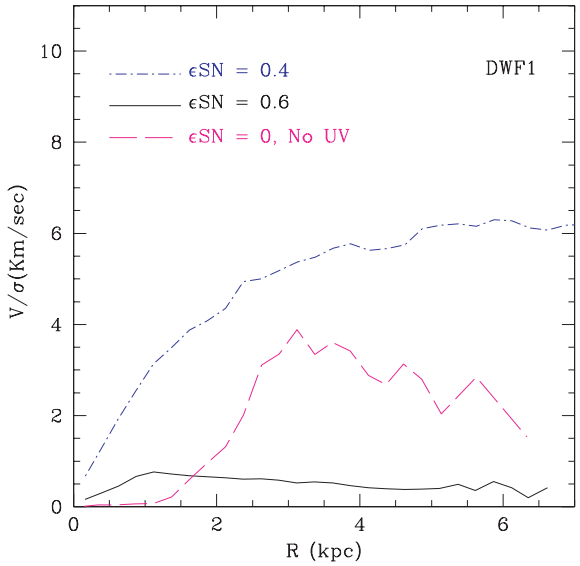

Figure 10. The V/σ ratio for the young stellar component of DWF1 as feedback is increased. Long dashed: no feedback or UV; dot dashed: ϵSN = 0.4; solid: ϵSN = 0.6.

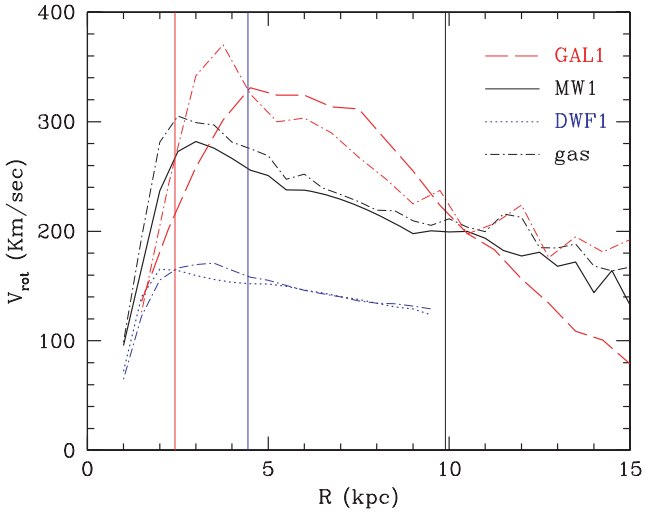

Figure 11. Azimuthally averaged rotation velocity of cold gas (dot–dashed line) and stars (age <4 Gyr). From top to bottom: GAL1, MW1, DWF1. The vertical lines show $2.2R_{\rm d}$ for each galaxy.

stars in the DWF1 run have $J/J_{\rm c} > 0.8$. 62 per cent of all stars in the MW1 galaxy have $J/J_{\rm c} > 0.8$. As a comparison most thin disc stars in the MW have $J/J_{\rm c} > 0.7$ (Nordström et al. 2004). A central hump in the $J/J_{\rm c}$ distribution that has often been interpreted as the sign of a massive halo/bulge component is evident in the DWF1 run. We verified that the low angular momentum stars are also the oldest, and were formed during DWF1's last major merger.

The amount of stellar rotation versus velocity dispersion, v/σ, is another good measure of how realistic are the discs that we obtained: $V_{\rm rot}/\sigma \sim 4$ for the MW1 disc stars younger than 4 Gyr, where σ is the rms average between the tangential and radial velocity dispersions. Typical observed values range from 2 to 5 for the discs of normal galaxies (Pizzella et al. 2004). Fig. 10 shows $V_{\rm rot}/\sigma$ for the young stellar component of DWF1. The dynamically coldest stellar disc is obtained with ϵSN = 0.4. Stronger feedback makes the ISM more turbulent, causing stars to form with a higher velocity dispersion. For all three galaxies runs without SN feedback generate stellar discs with lower $V_{\rm rot}/\sigma$ ratios, due to stronger loss of angular momentum driven by bar instabilities or because the velocity dispersion is increased by the overall stronger heating by satellites (that survive disruption much closer to the galaxy centre). These statements hold true irrespective of the selected age interval for the stars.

The azimuthally averaged rotation curves of galaxies are shown in Fig. 11. Both the rotation curve of the cold gas component and of the disc stars younger than 4 Gyr are plotted. For both the MW1 and DWF1 runs intermediate age stars and cold gas have very similar profiles, confirming that younger stars are in orbits close to circular. In the GAL1 run (our most massive galaxy), the stellar and gaseous discs are not completely coplanar. This offset creates a difference in the central part of the velocity profile of the two components. The outer part of GAL1's stellar disc is also dynamically hot, which makes $V_{\rm rot}$ of the stellar component decline very rapidly at outer radii.

While all our galaxies show long lasting bar instabilities, the introduction of SN feedback increases the stability of the disc and thus reduces the non-axisymmetry of the stellar disc. Stronger feedback generates stronger disc axisymmetry. In all simulations with feedback, only an oval distortion with scale smaller than the disc scalelength is present as opposed to a clear bar with scalelength $\sim$ disc scalelength in models without SN feedback. The small oval distortion is likely an unresolved bar, because our high-resolution control run (MW1hr) does display a resolved bar at its centre. Discs with feedback are more stable to bar formation because their stellar disc builds up more slowly over time.

We can understand the stabilizing effect of feedback by comparing the mass in the halo to that in the disc using the parameter $\varepsilon = (V_{\rm max} \times R_{\rm D})/GM_{\rm d}$, introduced by Efstathiou, Lake & Negroponte (1982) to measure the susceptibility of discs to bar formation. $V_{\rm max}$ is the peak circular velocity and $M_{\rm d}$ and $R_{\rm D}$ are, respectively, the mass and exponential scalelength of the disc. Numerical experiments (Efstathiou et al. 1982; Mayer & Wadsley 2004) show that $\varepsilon > \alpha$, with $0.95 < \alpha < 1.1$, is required for stability against bar formation of a disc of gas and stars (the higher the gas fraction, the higher α). Measuring ε in a cylinder within 0.5 kpc of the disc plane, we find that in the runs without feedback ε is already <0.9 at $z > 1$. In the runs with feedback, ε does not approach unity until near $z = 0$. In runs without feedback the disc is more massive and denser at earlier epochs, and thus more bar unstable. Without feedback, all the gas that is accreted rapidly makes disc stars, while with feedback a significant fraction of the baryons remain hot and diffuse and do not form stars even when they reach the disc. A visual comparison with real rotation curves shows that our simulated galaxies produce rotation curves that raise rapidly and then decline too fast at $R > 4\ R_{\rm d}$. Only DWF1 has a rotation curve close to being 'flat' as observed for most normal spiral galaxies (Catinella, Giovanelli & Haynes 2006). This is likely due to a combination of a still too massive central component and the outer part of discs being affected by two body heating from halo particles.

5.3 Gas-rich mergers and the formation of discs at high redshift

With our relatively high resolution we are able to follow the formation of discs early on in our simulations. Perhaps surprisingly, the disc of the MW1 galaxy starts forming immediately after the

last major merger event confirming early results by Elmegreen et al. (2005) and Springel & Hernquist (2005) that gas-rich mergers with substantial feedback are conducive to the observed early formation of discs (Trujillo et al. 2006). In our simulations feedback stops a substantial fraction of gas from turning into stars during the major merger. 40 per cent of the mass of the disc of MW1 is gas at $z = 2$. With lots of orbital angular momentum available from the merger, gas cools and rapidly settles into an extended exponential disc, especially in runs with stronger feedback and higher resolution. Even for DWF1 and GAL1, substantial stellar discs form immediately after $z_{\rm lmm}$. Without feedback a much more compact stellar component forms and becomes rapidly non-axisymmetric, as described in Section 5.2. At $z > 1$ stellar discs are 20–30 per cent larger when feedback is on, although by $z = 0$ their sizes are virtually identical. V/σ measured in the disc of the high resolution MW1hr run is $\sim$1.6 at $z = 1.5$ for stars that form shortly after $z_{\rm lmm}$. This stellar component is heated by a combination of the rapidly changing central potential and by a couple of minor satellite accretions on to the disc that occur before $z = 1.5$. This early disc could be associated with the thick disc components of present day spiral galaxies (Brook et al. 2004; Seth, Dalcanton & de Jong 2005; Yoachim & Dalcanton 2005).

5.4 Bulge and disc decomposition

To separate the bulge, disc and halo components we assigned to the 'bulge' all stars in the age range that would give a $V_{\rm rot}/\sigma < 1$ and within four disc vertical scaleheights from the disc plane. This selects an old, slowly rotating stellar component. Disc stars were those within four disc scaleheights and scalelengths that were not assigned to the bulge. Stars not belonging to the bulge, disc or individual satellites were assigned to the halo. The kinematically defined B/D mass ratio of the fiducial MW1 is $= 0.3$ or smaller. This result does not change for other reasonable decomposition techniques (Governato et al. 2004). We only used dynamical definitions of the galaxy components. A photometric decomposition was not attempted but given that stars in the discs are younger and then brighter it is likely that a luminosity-weighted estimate would give a lower B/D ratio. We speculate that the low B/D ratio of the MW1 is due to the high angular momentum acquired by cold gas during the last major merger event. The DWF1 and GAL1 simulations both formed a more massive 'bulge'. This result is likely a consequence of different physical processes: (i) the DWF1 galaxy has very low angular momentum (the last major merger at $z = 2.3$ is almost head-on); (ii) GAL1 forms stars in its central region until the present time, as gas keeps cooling from the surrounding halo. Its bulge has fairly blue colours and is relatively more massive. The relevant scalelengths are $<$1 kpc, so we decided to postpone a more detailed analysis of the bulge components of our simulated galaxies when higher resolution simulations will be available.

6 MATCHING THE TULLY–FISHER RELATION

The TF relation links the characteristic rotation velocity of a galaxy with its total absolute magnitude (Giovanelli et al. 1997). Similarly, the 'baryonic TF' relation (McGaugh et al. 2000; McGaugh 2005) links characteristic rotation velocity with total disc mass to account for the fact that less massive galaxies are more gas rich and thus that their stars only account for a small fraction of their disc total mass. Both relations imply that the total disc mass and its radial distribution are closely connected with the total mass of a halo. Early simulations matched the slope of the TF relation, but reported (Eke et al. 2001) difficulties in matching its normalization. The relatively weak feedback adopted in that work might have caused galaxies to cease SF relatively early, leaving the discs too red and then causing the TF relation offset. Alternatively, the central rotational velocities of the simulated galaxies were too high due to an excess of matter at the centre of galaxies possibly due to excessive baryonic cooling and the subsequent adiabatic contraction of the DM component. Even high-resolution simulations like Abadi et al. (2003) and Governato et al. (2004) have shown a consistent offset from the TF relation of late-type spirals, with galaxies being too centrally concentrated compared to real ones. Compared to some previous works our simulations have sufficient resolution to allow us a much direct comparison with observational data as $V_{\rm rot}$ is now measured at only a few kpc from the centre. This poses a much stronger constraint on simulations as they have to reproduce the stellar mass distribution and kinematics at relatively small scales.

When feedback is included, simulations successfully match both the TF and baryonic TF relations, this result being possibly the most important conclusion of the work presented here: it shows that our simulations produce a realistic distribution of stars, baryons and DM within the central few kpc. To compare our simulations with the observed TF relations, we used the rotation curves plotted in Fig. 9 (and described in Section 5.2) to determine $V_{\rm rot}$ measured at 3.5 disc scalelengths for DWF1, MW1 and GAL1 as in the Giovanelli sample. We then obtained the global magnitudes for each galaxy model by coupling the SFHs of our simulations with GRASIL (Silva et al. 1998), a code to compute the spectral evolution of stellar systems taking into account dust reprocessing. We considered each star particle as a single stellar population with the age, metallicity and mass assigned to it by the simulation. Stars with metallicities less than $Z = 0.0005$ were assigned that minimum value. GRASIL models the distribution of molecular clouds and dust based on the structural parameters of a galaxy disc and bulge. The quoted magnitudes in Table 5 are the average of different viewing angles.

Figs 12 and 13 show our galaxy models overplotted on TF and baryonic TF data from Giovanelli (private communication) and McGaugh (2005), respectively. The opposite residuals for DWF1 and MW1 from the average TF relation (continuous line in Fig. 11) correlate well with their halo spins: lower than average for DWF1 and higher for MW1. As GAL1 dynamical tracers are slightly decoupled (see Section 5.2), its location on the TF relations somewhat depends on the tracers chosen (old or young stars for the disc scalelength, stars or cold gas as tracer of the velocity field). As GAL1's stellar mass is larger than $10^{11}\,{\rm M}_{\odot}$ it is a likely candidate for an early spiral or even an S0. We speculate that another type of feedback, possibly from an active QSO at the bulge centre (Di Matteo et al. 2005; Hopkins et al. 2005), would decrease SF in the centre and lower the central gas density, reducing the relative weight of the central baryonic concentration.

Improvements in matching the TF and in conserving the angular momentum content of discs have been consistently reported in the literature as the robustness of simulations and the detail of physical modelling has continued to improve (Abadi et al. 2003; Sommer-Larsen et al. 2003; Governato et al. 2004; Robertson et al. 2004). As we show in Section 8 our simulations have a softening of the order of only 20 per cent of the disc scalelengths and give robust and likely converging results at scales corresponding to the typical scalelength of stellar discs. We verified that our match with the TF relations is not due to $V_{\rm rot} \ll V_{\rm c}$, i.e. the discs are not dynamically 'hot' within a few disc scalelengths and gas and young stars trace

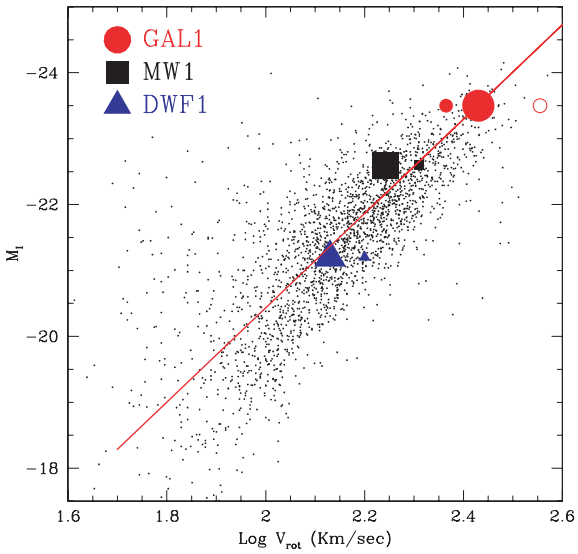

Figure 12. The TF relation using the data compilation from Giovanelli (private communication) and a fit to Giovanelli et al. (1997). Solid triangle: DWF1; solid square: MW1; solid dot: GAL1. Bigger dots shows $V_{\rm rot}$ measured at $3.5R_{\rm d}$. Smaller dots shows the effect of measuring $V_{\rm rot}$ at $2.2R_{\rm d}$. The small open dot uses $V_{\rm rot}$ measured from GAL1 cold gas component.

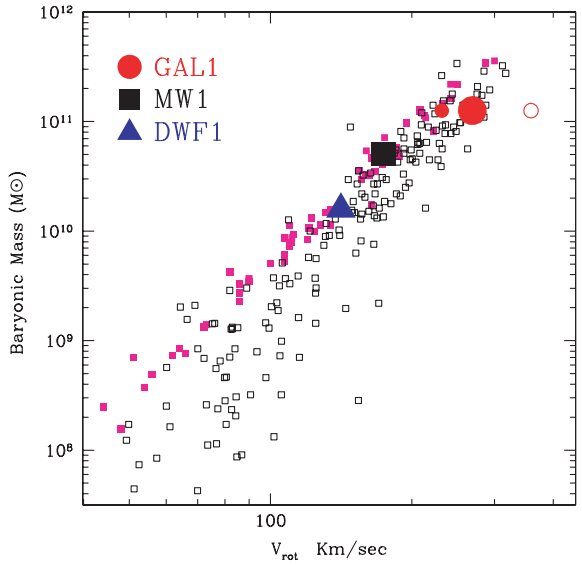

Figure 13. The baryonic TF relation. Squares show data points from (McGaugh 2005). $V_{\rm rot}$ is measured at $3.5R_{\rm d}$ (as in the observational sample) for each of the three galaxies. The two smaller points for the GAL1 run show the effect of measuring $V_{\rm rot}$ at $2.2R_{\rm d}$ using stars and the cold gas component, as shown in Fig. 12.

very closely the underlying potential. We verified that runs with no feedback produce galaxies slightly redder, but only in the *B* band and only for DWF1 where the effect is 0.3 mag with ϵSN = 0.4 and 0.5 mag for ϵSN = 0.6. For more massive galaxies and/or redder bands the effect is only 0.1–0.05 mag as the effect of feedback is smaller and SF happen mostly at higher redshifts. This small colour shift is not sufficient to explain the shift from the *I* band TF measured in some previous simulations.

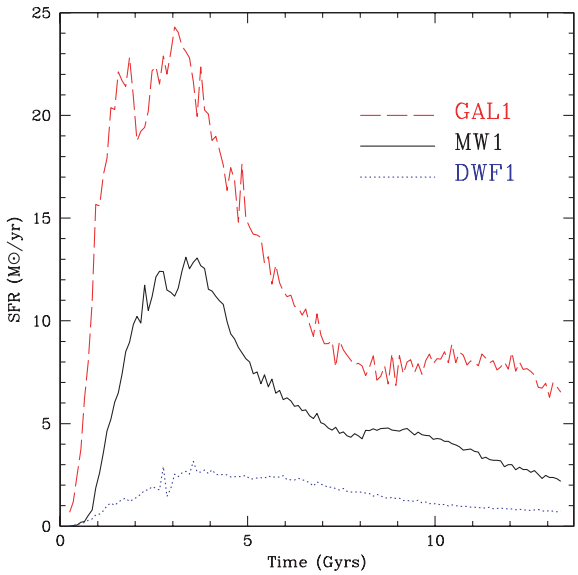

Figure 14. SFHs of DWF1, MW1 and GAL1, including all stars within four disc radial and vertical scaleheights. ϵSN = 0.4 and UV field on for all runs. Solid black: MW1; long dashed: GAL1; dotted: DWF1.

7 FEEDBACK AND THE STAR FORMATION HISTORIES OF GALAXIES

Not only does feedback affect the structure and stability of discs, as discussed in Sections 5.1 and 5.2, respectively, but we also expect it to shape their SFHs. The isolated test simulations of Section 2 hinted at this effect, and in this section we explore the effect of feedback on the SFHs of DWF1, MW1 and GAL1. The SFHs of bulge and disc stars in these three runs are shown in Fig. 14. The plot shows that the peak of SF is delayed in less massive haloes, as expected if feedback has a more pronounced effect in galaxies with shallower potential wells (Maller & Dekel 2002). To understand this result, consider the natural property of CDM models that SF at high redshift happens in a number of progenitors that eventually coalesce to form a present day galaxy. We used the DWF1 simulation to verify that increasing feedback limits the efficiency of SF in progenitor haloes with $V_{\rm c} < 30$–$50\,{\rm km\,s^{-1}}$ and delays it until small subhaloes merge into haloes with a sufficiently deep potential well (see also Neistein, van den Bosch & Dekel 2006).

To illustrate the crucial effect of feedback on the SFH of DWF1, Fig. 15 compares its SFH in the absence of feedback and with ϵSN = 0.6, the strongest feedback adopted in our study. Early SF is significantly reduced in the case of feedback, and we no longer see the initial strong starbursts evident in the run with no feedback. Lowering the efficiency of SF during mergers preserves a large quantity of cold gas that rapidly settled in rotationally supported discs. The run with feedback has a present day SFR almost 10 times higher than that without. The SFR in the run with feedback is far too low to match observations.

The $z = 0$ SFRs of DWF1, as well as of the other two galaxies, are quite similar to those observed in galaxies with the same stellar mass. Fig. 16 shows the $z = 0$ SFRs of our simulated galaxies overplotted with those measured for SDSS galaxies in a wide mass range (Brinchmann et al. 2004). Two low-mass field galaxies outside the virial radius of galaxy MW1 (but within the high-resolution region) have also been included to show a fair agreement between our theoretical model and observational data over more than two orders of magnitude in stellar mass.

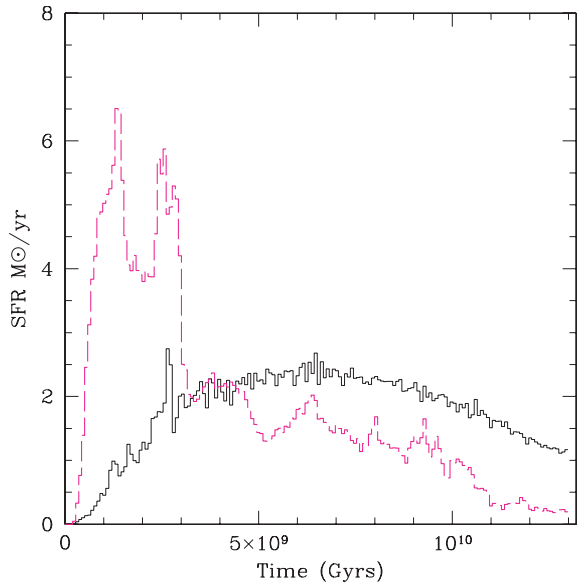

Figure 15. Galaxy DWF1: SFH including all stars within $4R_z$ and R_d from the disc plane for two runs. Solid line: ϵSN = 0.6; long dashed: no feedback, no UV. The addition of feedback smooths out the SF peaks otherwise present at high redshift and during the last major merger event at $z = 2.3$. Feedback delays the conversion of gas into stars until gas accumulates and cools in the potential well of the main progenitor.

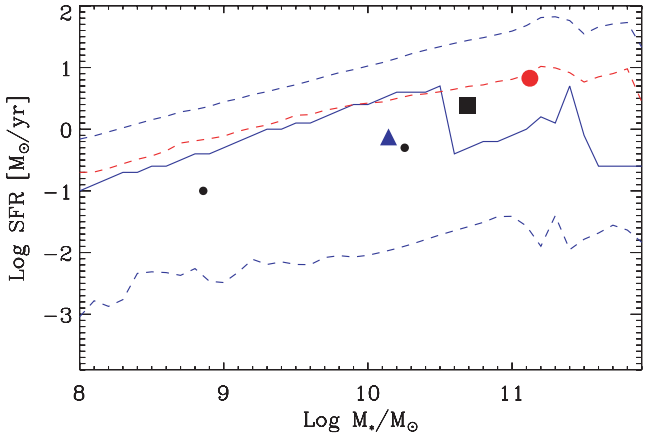

Figure 16. Present day SFR versus galaxy stellar mass for both simulated and observed galaxies. Triangle: DWF1; square: MW1; solid circle: GAL1. The two smaller dots are field galaxies in the high-resolution region of our simulations. The continuous line is the average SFR for the SDSS sample described in Brinchmann et al. (2004). The central dashed line is the median value. The upper and lower dashed lines include data three sigma from the mean of the observational sample.

Our galaxy models run with SN feedback also reproduce the observed 'downsizing' of field galaxies (Cowie et al. 1996; MacArthur et al. 2004): galaxies with a less massive stellar component are also younger. Fig. 17 shows that the inclusion of feedback and its differential effects at different galaxy masses naturally reproduces the observed trend: more massive galaxies also have older stellar populations. This trend disappears when runs with no feedback are considered (open circles) and average stellar ages correspond to the time of collapse of the first protogalaxies. As SN feedback removes baryons and delays SF in smaller haloes, it has a stronger

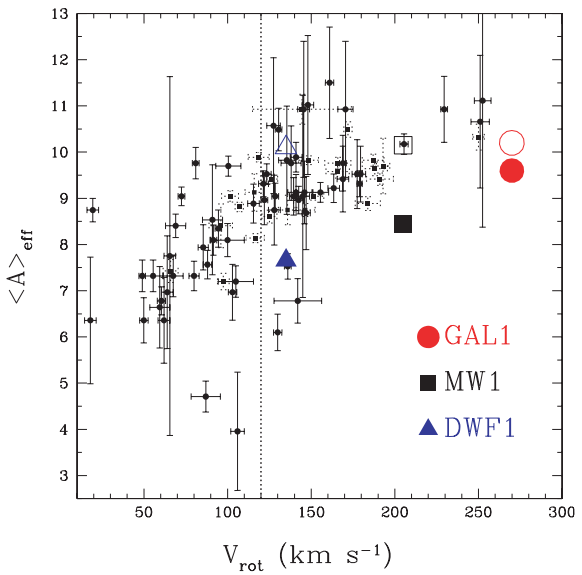

Figure 17. Mass weighted average age of stellar populations versus galaxy stellar mass. Small dots with error bars: from MacArthur et al. (2004). Solid large dots: simulations with ϵSN = 0.4. Open dots: simulations with no feedback or UV. V_{rot} is measured at 3.5 disc scalelengths.

effect in less massive galaxies that formed from even less massive progenitors at high redshift. Gas must collect inside a sufficiently deep potential well before it is able to cool efficiently. More massive galaxies are formed from the merging of more massive progenitors that were able to form stars already at high redshift. While CDM forms structure from the bottom up, the introduction of feedback reverses the trend for stellar populations.

Recently, Bell & de Jong (2001) and Conselice et al. (2005) used observations of spiral galaxies to measure the stellar mass associated with galaxies of different rotational velocities and halo mass. A comparison of our simulations with data in Conselice et al. (2005) and the best fit to Bell & de Jong (2001) is plotted in Fig. 18 and shows that our models form the right amount of stars in their bulge and

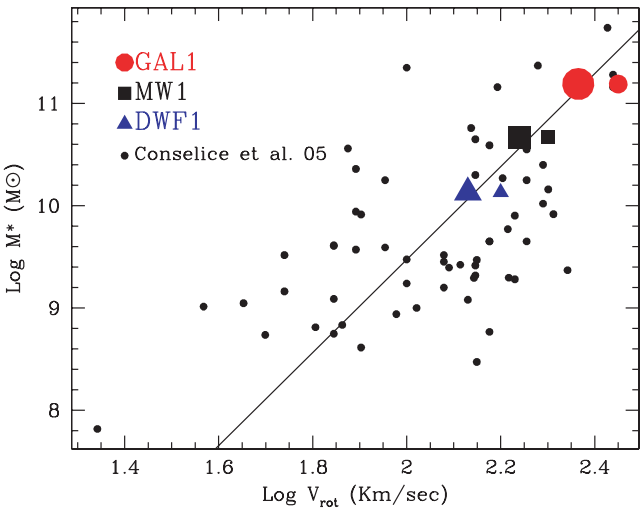

Figure 18. Total stellar mass versus rotational velocity. Solid small dots are data from Conselice et al. (2005). Large dots: simulations measured at $3.5R_d$. Small points: simulations measured at $2.2R_d$. The straight line is a fit from Bell & de Jong (2001).

disc components. We also verified that MW1 contains 4×10^{10} M$_\odot$ of DM within 8.5 kpc, again in good agreement with estimates for the MW (Eke et al. 2001). These results confirm that our modelling of SF and feedback created galaxies with the right amount of stars for their halo mass.

8 RESOLUTION TESTS: THE CENTRAL MASS PROFILE OF GALAXIES AND THE LUMINOSITY FUNCTION OF SATELLITES

In this section, we show that our results are robust to resolution effects. To do this, we have performed one additional simulation (MW1hr) to test if our results have converged as resolution is further increased. A more complete study on how resolution affects the formation of discs and the general properties of galaxies is highly needed but beyond the scope of this paper. MW1hr uses the same initial conditions as the MW1 runs, but uses eight times as many particles within the high-resolution region. ϵSN $= 0.6$ (as for run MW1g4) was used. Force resolution is improved by a factor of 2 to 0.3 kpc. Additional waves in the initial perturbations spectrum are consistently added. With a DM particle mass of only 7.6×10^5 M$_\odot$ and star particle mass of 3×10^4 M$_\odot$ this simulation has one of the highest resolutions for a MW-sized galaxy in a cosmological context to date. Because of its high computational cost we carried this simulation only to $z = 0.5$, using several tens of thousands of CPU (central processing unit) hours. Fig. 19 compares the circular velocity V_c of MW1g4 and MW1hr (again defined as $\sqrt{M(r < R)/R}$) for the DM, baryonic and stellar components, while Fig. 20 compares the V-band satellites LF (again at $z = 0.5$).

Fig. 19 shows that at the resolution of our standard runs the total mass profile and the quantity of stars have converged at radii corresponding to a couple of disc scalelengths. $V_{\rm rot}$ measured at $3.5R_{\rm D}$ (and used in Figs 12, 13, 17 and 18) is thus robust to resolution effects, at the resolution of our standard runs. Test runs in a cosmological context resolution (Governato et al., in preparation) show a systematic increase in V_c and a decrease of stellar $R_{\rm D}$ as resolution becomes increasingly worse. This result likely explains why our simulations match the normalization of the TF relation. However,

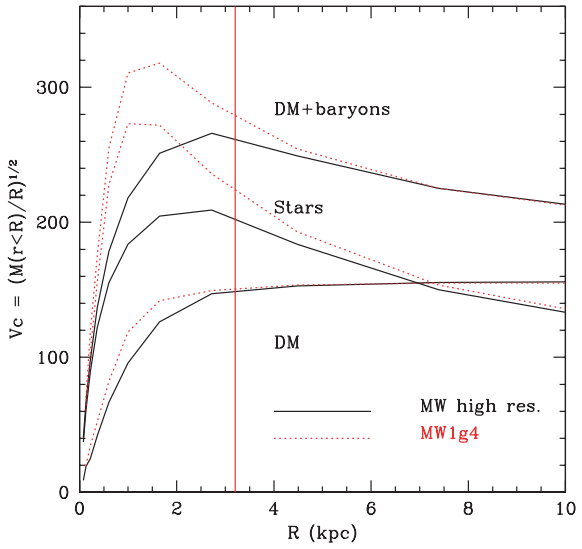

Figure 19. Resolution tests: the circular velocity $V_c = \sqrt{M(< R)/R}$ for run MW1hr (solid) and MW1g4 (dots). The mass distribution converges at radii larger than $r > 2.2R_{\rm d}$ (vertical line). The high resolution simulation contains significantly less baryons within a few times ϵ.

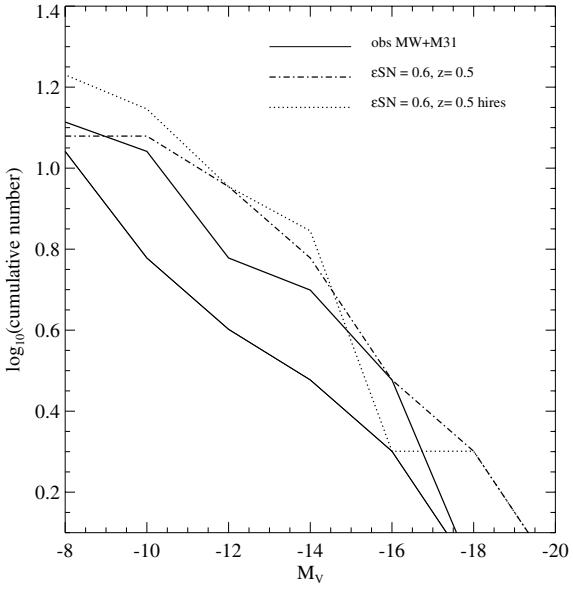

Figure 20. Resolution tests: the V-band LF of the satellites system of MW1g4 (dashed) and its high resolution version (dotted) at $z = 0.5$ compared with the MW and Andromeda (solid lines).

at smaller radii (only three–four times the gravitational softening) our standard run MW1g4 shows a much larger central mass than MW1hr. This unphysical mass concentration significantly raises the V_c such that it peaks at over 300 km s^{-1}. Because the standard and high-resolution runs adopted identical feedback and SF parameters, this result shows that resolution plays an important role in the central region of galaxies. In DM only simulations, low resolution artificially lowers central DM densities. In contrast with DM only simulations, low resolution and lack of feedback in SPH simulations causes baryons to become more centrally concentrated due to partially artificial angular momentum loss. As resolution is increased, reduced artificial angular momentum loss by both the stellar and gaseous component allow SN feedback to be more effective and to reduce the central baryon concentration. Worse resolution and possibly weaker feedback would have overestimated the amount of baryons within 2.2 $R_{\rm d}$. As the force resolution is increased the disc bar instability in the disc of MW1hr starts earlier ($z \sim 2$) and is more pronounced than in the MW1g4 simulation, confirming studies by Kaufmann et al. (2006b). At this high resolution the fraction of cold baryons is 40 per cent higher, and the mass in stars is only 5 per cent lower. We also begin to resolve the thermal instabilities predicted by Maller & Bullock (2004) and recently detected in simulations of isolated galaxies (Kaufmann et al. 2006a). It is encouraging that the satellite V-band LF (Fig. 20) remains substantially unaltered as resolution is increased, although a few more satellites as faint as $M_V = -8$ are now resolved. This supports results from S06 that our adopted SF + SN algorithm is relatively insensitive to resolution.

9 CONCLUSIONS

We have presented a new set of simulations of the formation of disc-dominated galaxies in a full ΛCDM cosmological context carried to the present time. These simulations included a simple but physically motivated recipe for SF. We used isolated galaxy models to calibrate the free parameters of our SF/feedback scheme to reproduce several important properties of the stellar and ISM components of local

disc galaxies over a range of masses. We then used this SF/feedback algorithm in cosmological simulations with no further adjustment.

We simulated three different haloes in a cosmological context, with masses typical of those associated with disc galaxies. These cosmological simulations have a very high number of resolution elements within the virial radius of the simulated galaxies ($\sim 1.5 \times 10^5$ for each of the DM and gas components and a few hundred thousand star particles), allowing us to resolve individual satellites down to $V_c \sim 20$ per cent of the parent galaxy. A rotation-dominated stellar disc galaxy with a significant exponential component naturally forms within each of these haloes. Our MW1 simulation provides a good example of how the stellar disc can form shortly after a major merger event, due to the large amount of orbital angular momentum transferred to the gas component during the merger event. Our three simulated galaxies (DWF1, MW1, GAL1) share the size, stellar mass, colours and current SFR typical of a low-mass galaxy, of a MW-like galaxy and a massive early-type spiral, respectively.

One of our most significant results is that the simulated galaxies fall on the TF and baryonic TF relations. This match is possible in part due to the high resolution of the simulations: resolution is crucial to avoid artificially losing the angular momentum gained this way (Governato et al. 2004; Kaufmann et al. 2006b). At our resolution, rotation curves have been resolved down to a fraction of the stellar disc scalelengths and (measured at 3.5 R_d) range from 135 to 270 km s^{-1} in amplitude. The MW-sized galaxy contains an amount of DM within the solar radius well in agreement with observational constraints. The simulated galaxies also reproduced the observed 'antihierarchical' trend of stellar populations: smaller galaxies have younger stellar populations. As feedback delays SF in protogalaxies a larger reservoir of gas remains available to form discs until the bulk of the mass of galaxy is assembled, typically between redshift 3 and 1. Feedback and the cosmic UV field also drastically reduce the number of galaxy satellites containing a significant stellar population.

We have complemented our standard runs with a high-resolution test run of our MW-sized halo. This run has and unprecedented number of particles: several million within R_{vir}. We used it to test the convergence of results in our standard runs. At our highest resolution the main galaxy is significantly less centrally concentrated, reducing its bulge mass and its peak velocity considerably. While stellar bulges are likely still unresolved in our standard runs, our tests and estimates from previous works suggest that the mass distribution and the rotation velocity of the cold gas and young stellar components have converged at the scales of a few kpc. Such a high resolution coupled with a physically motivated description of feedback explains why our models do indeed fall on to the TF relations.

These simulations and those published in the recent literature show that some significant progress has been done toward understanding galaxy formation in the context of a ΛCDM concordance cosmology. However, areas remain were progress needs to be made: (i) a larger range of initial conditions needs to be explored to understand the role played by halo spin and merging history on the morphology and colours of galaxies; (ii) our resolution test shows that the inner mass distribution of the galaxies, including the bulge, is still poorly resolved by our standard runs and that possibly several million resolution elements per galaxy are needed to approach convergence; (iii) satellites are still too bright compared to those orbiting our MW. While cosmic variance likely played a role [the largest satellites accreted by the MW1 system is more massive than the Large Magellanic Cloud (LMC)], one obvious possibility to create fainter satellites would be to increase the efficiency of SN feedback, but that needs to be carefully calibrated with the other constraints. Two intriguing possibilities that we plan to explore in future works are the increased feedback and UV field due to massive Population III stars (Choudhury & Ferrara 2005) and the local proximity effect that SF from the main galaxy might have on the nearby dwarfs (Gnedin 2000). Overall, the possibility of obtaining a good match to the observed satellite LF seems within reach of future simulations.

ACKNOWLEDGMENTS

FG would like to thank A. Dekel, E. D'Onghia, T. Kaufmann, J. Silk and M. Steinmetz for helpful conversations during this project. We thank J. Brinchmann, C. Conselice, S. McGaugh, L. MacArthur and R. Giovanelli for sharing their data with us. Support for this work, part of the Spitzer Space Telescope Theoretical Research Program, was provided by NASA through a contract issued by the Jet Propulsion Laboratory, California Institute of Technology under a contract with NASA. FG was a Brooks Fellow during the initial stages of this project and was supported in part by NSF grants AST-0098557 and AST-61-3931. TQ acknowledges support from NSF grant AST-0098557 and NSF grant PHY-0205413. Most simulations were run at the Arctic Region Supercomputing Center and on a local SGI multi-CPU machine.

REFERENCES

Abadi M. G., Navarro J. F., Steinmetz M., Eke V. R., 2003, ApJ, 591, 499
Balogh M. L., Pearce F. R., Bower R. G., Kay S. T., 2001, MNRAS, 326, 1228
Balsara D. S., 1997, in Clarke D. A., West M. J., eds, ASP Conf. Ser. Vol. 123, Computational Astrophysics. Astron. Soc. Pac., San Francisco, p. 274
Bardeen J. M., Bond J. R., Kaiser N., Szalay A. S., 1986, ApJ, 304, 15
Barnes J. E., Hernquist L., 1996, ApJ, 471, 115
Baugh C. M., Cole S., Frenk C. S., 1996, MNRAS, 283, 1361
Bell E. F., de Jong R. S., 2001, ApJ, 550, 212
Benson A. J., Frenk C. S., Lacey C. G., Baugh C. M., Cole S., 2002, MNRAS, 333, 177
Benz W., 1990, in Buchler J. R., ed., Numerical Modelling of Nonlinear Stellar Pulsations Problems and Prospects. Kluwer Academic Publishers, Dordrecht, p. 269
Binney J., Gerhard O., Silk J., 2001, MNRAS, 321, 471
Bizyaev D., Mitronova S., 2002, A&A, 389, 795
Blanton M. R. et al., 2003, ApJ, 594, 186
Blumenthal G. R., Faber S. M., Primack J. R., Rees M. J., 1984, Nat, 311, 517
Brinchmann J., Charlot S., White S. D. M., Tremonti C., Kauffmann G., Heckman T., Brinkmann J., 2004, MNRAS, 351, 1151
Broeils A. H., Rhee M.-H., 1997, A&A, 324, 877
Brook C. B., Kawata D., Gibson B. K., Freeman K. C., 2004, ApJ, 612, 894
Bundy K., Ellis R., Conselice C., 2005, ApJ, 625, 621
Catinella B., Giovanelli R., Haynes M. P., 2006, ApJ, 640, 751
Cen R., Ostriker J. P., 1999, ApJ, 514, 1
Choudhury T. R., Ferrara A., 2005, MNRAS, 361, 577
Cole S., Lacey C. G., Baugh C. M., Frenk C. S., 2000, MNRAS, 319, 168
Conselice C. J., Bundy K., Ellis R. S., Brichmann J., Vogt N. P., Phillips A. C., 2005, ApJ, 628, 160
Cowie L. L., Songaila A., Hu E. M., Cohen J. G., 1996, AJ, 112, 839
Davis M., Efstathiou G., Frenk C. S., White S. D. M., 1985, ApJ, 292, 371
Debattista V. P., Carollo C. M., Mayer L., Moore B., 2004, ApJ, 604, L93
Debattista V. P., Mayer L., Carollo C. M., Moore B., Wadsley J., Quinn T., 2006, ApJ, 645, 209
Dekel A., Woo J., 2003, MNRAS, 344, 1131
Diemand J., Moore B., Stadel J., Kazantzidis S., 2004, MNRAS, 348, 977
Di Matteo T., Springel V., Hernquist L., 2005, Nat, 433, 604

D'Onghia E., Burkert A., Murante G., Khochfar S., 2006, MNRAS, 372, 1525
Efstathiou G., 2000, MNRAS, 317, 697
Efstathiou G., Lake G., Negroponte J., 1982, MNRAS, 199, 1069
Eke V., Efstathiou G., Wright L., 2000, MNRAS, 315, L18
Eke V. R., Navarro J. F., Steinmetz M., 2001, ApJ, 554, 114
Elmegreen B. G., Elmegreen D. M., Vollbach D. R., Foster E. R., Ferguson T. E., 2005, ApJ, 634, 101
Evrard A. E., 1988, MNRAS, 235, 911
Fall S. M., 1983, in Athanassoula E., ed., Proc. IAU Symp. 100, Internal Kinematics and Dynamics of Galaxies. Reidel, Dordrecht, p. 391
Fall S. M., Efstathiou G., 1980, MNRAS, 193, 189
Ferrara A., 2002, in Grebel E. K., Brandner W., eds, ASP Conf. Ser. Vol. 285, Modes of Star Formation and the Origin of Field Populations. Astron. Soc. Pac., San Francisco, p. 367
Ferreras I., Silk J., Böhm A., Ziegler B., 2004, MNRAS, 355, 64
Florido E., Battaner E., Guijarro A., Garzón F., Jiménez-Vicente J., 2001, A&A, 378, 82
Frenk C. S., White S. D. M., Efstathiou G., Davis M., 1985, Nat, 317, 595
Gallazzi A., Charlot S., Brinchmann J., White S. D. M., Tremonti C. A., 2005, MNRAS, 362, 41
Gardner J. P., 2001, ApJ, 557, 616
Gerritsen J. P. E., 1997, PhD thesis, Univ. Groningen
Gilmore G., Wyse R. F. G., Norris J. E., 2002, ApJ, 574, L39
Giovanelli R., Haynes M. P., Herter T., Vogt N. P., da Costa L. N., Freudling W., Salzer J. J., Wegner G., 1997, AJ, 113, 53
Gnedin N. Y., 2000, ApJ, 535, 530
Governato F., Moore B., Cen R., Stadel J., Lake G., Quinn T., 1997, New Astron., 2, 91
Governato F. et al., 2004, ApJ, 607, 688
Granato G. L., De Zotti G., Silva L., Bressan A., Danese L., 2004, ApJ, 600, 580
Haardt F., Madau P., 1996, ApJ, 461, 20
Haehnelt M. G., Steinmetz M., Rauch M., 1998, ApJ, 495, 647
Hopkins P. F., Hernquist L., Cox T. J., Di Matteo T., Martini P., Robertson B., Springel V., 2005, ApJ, 630, 705
Katz N., 1992, ApJ, 391, 502
Katz N., White S. D. M., 1993, ApJ, 412, 455
Katz N., Weinberg D. H., Hernquist L., 1996, ApJS, 105, 19
Kaufmann T., Mayer L., Moore B., Stadel J., Wadsley J., 2006a, MNRAS, 370, 1612
Kaufmann T. et al., 2006b, MNRAS, in press (doi:10.1111/j.1365-2966.2006.11314.x) (astro-ph/0601115)
Kawata D., Arimoto N., Cen R., Gibson B., 2006, ApJ, 641, 785
Kennicutt R. C., 1998, ApJ, 498, 541
Klypin A., Kravtsov A. V., Valenzuela O., Prada F., 1999, ApJ, 522, 82
Klypin A., Zhao H., Somerville R. S., 2002, ApJ, 573, 597
Kormendy J., Kennicutt R. C., 2004, ARA&A, 42, 603
Kravtsov A. V., Gnedin O. Y., 2005, ApJ, 623, 650
Kravtsov A. V., Gnedin O. Y., Klypin A. A., 2004, ApJ, 609, 482
Krumholz M., McKee C., 2005, ApJ, 630, 250
Lake G., Carlberg R. G., 1988, AJ, 96, 1587
Li Y., Mo H., van den Bosch F., 2005, MNRAS, submitted (astro-ph/0510372)
MacArthur L. A., Courteau S., Bell E., Holtzman J. A., 2004, ApJS, 152, 175
Macciò A. V., Governato F., Horellou C., 2005, MNRAS, 359, 941
McGaugh S. S., 2005, ApJ, 632, 859
McGaugh S. S., Schombert J. M., Bothun G. D., de Blok W. J. G., 2000, ApJ, 533, L99
McKee C. F., Ostriker J. P., 1977, ApJ, 218, 148
Mac Low M., Ferrara A., 1999, ApJ, 513, 142
Maller A. H., Bullock J. S., 2004, MNRAS, 355, 694
Maller A. H., Dekel A., 2002, MNRAS, 335, 487
Martin C. L., 1999, ApJ, 513, 156
Martin D. C. et al., 2005, ApJ, 619, L1
Mateo M. L., 1998, ARA&A, 36, 435
Mayer L., Moore B., 2004, MNRAS, 354, 477
Mayer L., Wadsley J., 2004, MNRAS, 347, 277
Mo H. J., Miralda-Escude J., 1996, ApJ, 469, 589
Monaco P., 2004, MNRAS, 352, 181
Monaghan J. J., 1992, ARA&A, 30, 543
Moore B., Governato F., Quinn T., Stadel J., Lake G., 1998, ApJ, 499, L5
Moore B., Ghigna S., Governato F., Lake G., Quinn T., Stadel J., Tozzi P., 1999, ApJ, 524, L19
Navarro J. F., Steinmetz M., 1997, ApJ, 478, 13
Navarro J. F., Steinmetz M., 2000, ApJ, 538, 477
Navarro J. F., White S. D. M., 1994, MNRAS, 267, 401
Neistein E., van den Bosch F. C., Dekel A., 2006, MNRAS, 372, 933
Nordström B. et al., 2004, A&A, 418, 989
Okamoto T., Eke V. R., Frenk C. S., Jenkins A., 2005, MNRAS, 363, 1299
Ostriker J. P., McKee C. F., 1988, Rev. Mod. Phys., 60, 1
Peebles P. J. E., 1969, ApJ, 155, 393
Peebles P. J., Ratra B., 2003, Rev. Mod. Phys., 75, 559
Perlmutter S. et al., 1997, ApJ, 483, 565
Pizzella A., Corsini E. M., Vega Beltrán J. C., Bertola F., 2004, A&A, 424, 447
Pohlen M., Balcells M., Lütticke R., Dettmar R.-J., 2004, A&A, 422, 465
Power C., Navarro J. F., Jenkins A., Frenk C. S., White S. D. M., Springel V., Stadel J., Quinn T., 2003, MNRAS, 338, 14
Quinn T., Katz N., Efstathiou G., 1996, MNRAS, 278, L49
Raiteri C. M., Villata M., Navarro J. F., 1996, A&A, 315, 105
Robertson B., Yoshida N., Springel V., Hernquist L., 2004, ApJ, 606, 32
Ryder S. D., Dopita M. A., 1994, ApJ, 430, 142
Seth A. C., Dalcanton J. J., de Jong R. S., 2005, AJ, 129, 1331
Shen S., Mo H. J., White S. D. M., Blanton M. R., Kauffmann G., Voges W., Brinkmann J., Csabai I., 2003, MNRAS, 343, 978
Silk J., 2001, MNRAS, 324, 313
Silva L., Granato G. L., Bressan A., Danese L., 1998, ApJ, 509, 103
Slyz A. D., Devriendt J. E. G., Bryan G., Silk J., 2005, MNRAS, 356, 737
Sommer-Larsen J., Götz M., Portinari L., 2003, ApJ, 596, 47
Spergel D. N. et al., 2003, ApJS, 148, 175
Springel V., 2000, MNRAS, 312, 859
Springel V., Hernquist L., 2002, MNRAS, 333, 649
Springel V., Hernquist L., 2005, ApJ, 622, L9
Steinmetz M., Navarro J. F., 2002, New Astron., 7, 155
Stinson G., Seth A., Katz N., Governato F., Wadsley J., Quinn T., 2006, MNRAS, 373, 1074 (S06)
Tasker E. J., Bryan G., 2006, ApJ, 641, 878
Thacker R. J., Couchman H. M. P., 2000, ApJ, 545, 728
Tittley E. R., Pearce F. R., Couchman H. M. P., 2001, ApJ, 561, 69
Toomre A., Toomre J., 1972, ApJ, 178, 623
Trujillo I., Pohlen M., 2005, ApJ, 630, L17
Trujillo I. et al., 2006, ApJ, 650, 18
Valenzuela O., Klypin A., 2003, MNRAS, 345, 406
Wada K., Norman C. A., 2001, ApJ, 547, 172
Wadsley J. W., Stadel J., Quinn T., 2004, New Astron., 9, 137
West A. A., Garcia-Appadoo D. A., Dalcanton J. J., Disney M. J., 2005, in Popescu C. C., Tuffs R. J., eds, AIP Conf. Proc. 761, The Spectral Energy Distributions of Gas-Rich Galaxies: Confronting Models with Data. Am. Inst. Phys., New York, p. 409
White S. D. M., Frenk C. S., 1991, ApJ, 379, 52
White S. D. M., Rees M. J., 1978, MNRAS, 183, 341
Willman B., Governato F., Dalcanton J. J., Reed D., Quinn T., 2004, MNRAS, 353, 639
Yepes G., Kates R., Khokhlov A., Klypin A., 1997, MNRAS, 284, 235
Yoachim P., Dalcanton J. J., 2005, ApJ, 624, 701
Yoachim P., Dalcanton J. J., 2006, AJ, 131, 226
Zaldarriaga M., Seljak U., 2000, ApJS, 129, 431

This paper has been typeset from a TEX/LATEX file prepared by the author.